International Journal of Modern Physics E

PRIMORDIAL NUCLEOSYNTHESIS: SUCCESSES AND CHALLENGES

GARY STEIGMAN

Physics Department, The Ohio State University, 191 West Woodruff Avenue Columbus, Ohio 43210, USA

Received 15 November 2005

Primordial nucleosynthesis provides a probe of the Universe during its early evolution. Given the progress exploring the constituents, structure, and recent evolution of the Universe, it is timely to review the status of Big Bang Nucleosynthesis (BBN) and to confront its predictions, and the constraints which emerge from them, with those derived from independent observations of the Universe at much later epochs in its evolution. Following an overview of the key physics controlling element synthesis in the early Universe, the predictions of the standard models of cosmology and particle physics are presented, along with those from some non-standard models. The observational data used to infer the primordial abundances are described, with an emphasis on the distinction between *precision* and *accuracy*. These relic abundances are compared with predictions, testing the internal consistency of BBN and enabling a comparison of the BBN constraints with those derived from the WMAP Cosmic Background Radiation data. Emerging from these comparisons is a successful standard model along with constraints on (or hints of) physics beyond the standard models of particle physics and of cosmology.

Keywords: Big Bang Nucleosynthesis; Early Universe Expansion Rate; Neutrino Asymmetry; Abundances of D, ^{3}He, ^{4}He, ^{7}Li.

1. Introduction

As the Universe evolved from its early, hot, dense beginnings (the "Big Bang") to its present, cold, dilute state, it passed through a brief epoch when the temperature (average thermal energy) and density of its nucleon component were such that nuclear reactions building complex nuclei could occur. Because the nucleon content of the Universe is small (in a sense to be described below) and because the Universe evolved through this epoch very rapidly, only the lightest nuclides (D, ^{3}He, ^{4}He, and ^{7}Li) could be synthesized in astrophysically interesting abundances. The relic abundances of these nuclides provide probes of conditions and contents of the Universe at a very early epoch in its evolution (the first few minutes) otherwise hidden from our view. The standard model of Cosmology subsumes the standard model of particle physics (*e.g.*, three families of very light, left-handed neutrinos along with their right-handed antineutrinos) and uses General Relativity (*e.g.*, the Friedman equation) to track the time-evolution of the universal expansion rate and

its matter and radiation contents. While nuclear reactions among the nucleons are always occurring in the early Universe, Big Bang Nucleosynthesis (BBN) begins in earnest when the Universe is a few minutes old and it ends less than a half hour later when nuclear reactions are quenched by low temperatures and densities. The BBN abundances depend on the conditions (temperature, nucleon density, expansion rate, neutrino content and neutrino-antineutrino asymmetry, etc.) at those times and are largely independent of the detailed processes which established them. As a consequence, BBN can test and constrain the parameters of the standard model (SBBN), as well as probe any non-standard physics/cosmology which changes those conditions.

The relic abundances of the light nuclides synthesized in BBN depend on the competition between the nucleon density-dependent nuclear reaction rates and the universal expansion rate. In addition, while all primordial abundances depend to some degree on the initial (when BBN begins) ratio of neutrons to protons, the ^{4}He abundance is largely fixed by this ratio, which is determined by the competition between the weak interaction rates and the universal expansion rate, along with the magnitude of any $\nu_e - \bar{\nu}_e$ asymmetry.[a] To summarize, in its simplest version BBN depends on three unknown parameters: the baryon asymmetry; the lepton asymmetry; the universal expansion rate. These parameters are quantified next.

1.1. *Baryon Asymmetry – Nucleon Abundance*

In the very early universe baryon-antibaryon pairs (quark-antiquark pairs) were as abundant as radiation (*e.g.*, photons). As the Universe expanded and cooled, the pairs annihilated, leaving behind any baryon **excess** established during the earlier evolution of the Universe[1]. Subsequently, the number of baryons in a comoving volume of the Universe is preserved. After $e^{\pm}$ pairs annihilate, when the temperature (in energy units) drops below the electron mass, the number of Cosmic Background Radiation (CBR) photons in a comoving volume is also preserved. As a result, it is useful (and conventional) to measure the universal baryon asymmetry by comparing the number of (*excess*) baryons to the number of photons in a comoving volume (post-$e^{\pm}$ annihilation). This ratio defines the baryon abundance parameter $\eta_{\rm B}$,

$$\eta_{\rm B} \equiv \frac{n_{\rm B} - n_{\bar{\rm B}}}{n_\gamma}. \tag{1}$$

As will be seen from BBN, and as is confirmed by a variety of independent (non-BBN), astrophysical and cosmological data, $\eta_{\rm B}$ is very small. As a result, it is convenient to introduce $\eta_{10} \equiv 10^{10}\eta_{\rm B}$ and to use it as one of the adjustable parameters for BBN. An equivalent measure of the baryon density is provided by the baryon density parameter, $\Omega_{\rm B}$, the ratio (at present) of the baryon mass density to

[a] A lepton asymmetry much larger than the baryon asymmetry (which is very small; see §1.1 below) would have to reside in the neutrinos since charge neutrality ensures that the electron-positron asymmetry is comparable to the baryon asymmetry.

the critical density. In terms of the present value of the Hubble parameter (see §1.2 below), $H_0 \equiv 100h$ km s^{-1} Mpc^{-1}, these two measures are related by

$$\eta_{10} \equiv 10^{10}(n_{\rm B}/n_\gamma)_0 = 274\Omega_{\rm B}h^2. \tag{2}$$

Note that the subscript 0 refers to the present epoch (redshift $z = 0$).

From a variety of non-BBN cosmological observations whose accuracy is dominated by the very precise CBR temperature fluctuation data from WMAP[2], the baryon abundance parameter is limited to a narrow range centered near $\eta_{10} \approx 6$. As a result, while the behavior of the BBN-predicted relic abundances will be described qualitatively as functions of $\eta_{\rm B}$, for quantitative comparisons the results presented here will focus on the limited interval $4 \leq \eta_{10} \leq 8$. As will be seen below (§2.2), over this range there are very simple, yet accurate, analytic fits to the BBN-predicted primordial abundances.

1.2. *The Expansion Rate At BBN*

For the standard model of cosmology, the Friedman equation relates the expansion rate, quantified by the Hubble parameter (H), to the matter-radiation content of the Universe.

$$H^2 = \frac{8\pi}{3} G_{\rm N} \rho_{\rm TOT}, \tag{3}$$

where $G_{\rm N}$ is Newton's gravitational constant. During the early evolution of the Universe the total density, $\rho_{\rm TOT}$, is dominated by "radiation" (*i.e.*, by the contributions from massless and/or extremely relativistic particles). During radiation dominated epochs (RD), the age of the Universe (t) and the Hubble parameter are simply related by $(Ht)_{\rm RD} = 1/2$.

Prior to BBN, at a temperature of a few MeV, the standard model of particle physics determines that the relativistic particle content consists of photons, $e^\pm$ pairs and three flavors of left-handed (*i.e.*, one helicity state) neutrinos (along with their right-handed, antineutrinos; $\rm N_\nu = 3$). With all chemical potentials set to zero (very small lepton asymmetry) the energy density of these constituents in thermal equilibrium is

$$\rho_{\rm TOT} = \rho_\gamma + \rho_e + 3\rho_\nu = \frac{43}{8}\rho_\gamma, \tag{4}$$

where ρ_γ is the energy density in the CBR photons (which have redshifted to become the CBR photons observed today at a temperature of 2.7K). In this case (SBBN: $\rm N_\nu = 3$), the time-temperature relation derived from the Friedman equation is,

$$\rm Pre-e^\pm \ annihilation: \quad t\, T_\gamma^2 = 0.738\ MeV^2\ s. \tag{5}$$

In SBBN it is usually assumed that the neutrinos are fully decoupled prior to $e^\pm$ annihilation; if so, they don't share in the energy transferred from the annihilating $e^\pm$ pairs to the CBR photons. In this very good approximation, the pho-

tons are hotter than the neutrinos in the post-$e^{\pm}$ annihilation universe by a factor $T_\gamma/T_\nu = (11/4)^{1/3}$, and the total energy density is

$$\rho_{\rm TOT} = \rho_\gamma + 3\rho_\nu = 1.68\rho_\gamma, \tag{6}$$

corresponding to a modified time-temperature relation,

$$\text{Post} - \text{e}^{\pm}\ \text{annihilation}: \quad t\ T_\gamma^2 = 1.32\ \text{MeV}^2\ \text{s}. \tag{7}$$

Quite generally, new physics beyond the standard models of cosmology or particle physics could lead to a non-standard, early Universe expansion rate (H'), whose ratio to the standard rate (H) may be parameterized by an expansion rate factor S,

$$H \to H' \equiv SH. \tag{8}$$

A non-standard expansion rate might originate from modifications to the 3+1 dimensional Friedman equation as in some higher dimensional models[3], or from a change in the strength of gravity[4]. Different gravitational couplings for fermions and bosons[5] would have similar effects. Alternatively, changing the particle population in early Universe will modify the energy density – temperature relation, also leading, through eq. 3, to $S \neq 1$. While these different mechanisms for implementing a non-standard expansion rate are not necessarily equivalent, specific models generally lead to specific predictions for S.

Consider, for example, the case of a non-standard energy density.

$$\rho_{\rm R} \to \rho'_{\rm R} \equiv S^2\rho_{\rm R}, \tag{9}$$

where $\rho'_{\rm R} = \rho_{\rm R} + \rho_X$ and X identifies the non-standard component. With the restriction that the X are relativistic, this extra component, non-interacting at $e^{\pm}$ annihilation, behaves as would an additional neutrino flavor. It must be emphasized that X is **not** restricted to additional flavors of active or sterile neutrinos. In this class of models S is constant prior to $e^{\pm}$ annihilation and it is convenient (and conventional) to account for the extra contribution to the standard-model energy density by normalizing it to that of an "equivalent" neutrino flavor[6], so that

$$\rho_X \equiv \Delta N_\nu \rho_\nu = \frac{7}{8}\Delta N_\nu \rho_\gamma. \tag{10}$$

For this case,

$$S \equiv S_{pre} = \left(1 + \frac{7}{43}\Delta N_\nu\right)^{1/2}. \tag{11}$$

In another class of non-standard models the early Universe is heated by the decay of a massive particle, produced earlier in the evolution[7]. If the Universe is heated to a temperature which is too low to (re)populate a thermal spectrum of the standard neutrinos ($T_{\rm RH} \lesssim 7$ MeV), the effective number of neutrino flavors contributing to the total energy density is < 3, resulting in $\Delta N_\nu < 0$ and $S < 1$.

Since the expansion rate is more fundamental than is ΔN_ν, BBN for models with non-standard expansion rates will be parameterized using S (but, for comparison, the corresponding value of ΔN_ν from eq. 11 will often be given for comparison). The simple, analytic fits to BBN presented below (§2.2) are quite accurate for $0.85 \leq S \leq 1.15$, corresponding to $-1.7 \lesssim \Delta\mathrm{N}_\nu \lesssim 2.0$

1.3. *Neutrino Asymmetry*

The baryon asymmetry of the Universe, quantified by $\eta_{\rm B}$, is very small. If, as expected in the currently most popular particle physics models, the universal lepton and baryon numbers are comparable, then any asymmetry between neutrinos and antineutrinos ("neutrino degeneracy") will be far too small to have a noticeable effect on BBN. However, it is possible that the baryon and lepton asymmetries are disconnected and that the lepton (neutrino) asymmetry could be large enough to perturb the SBBN predictions. In analogy with $\eta_{\rm B}$ which quantifies the baryon asymmetry, the lepton (neutrino) asymmetry, $L = L_\nu \equiv \Sigma_\alpha L_{\nu_\alpha}$, may be quantified by the neutrino chemical potentials μ_{ν_α} ($\alpha \equiv e, \mu, \tau$) or, by the degeneracy parameters, the ratios of the neutral lepton chemical potentials to the temperature (in energy units) $\xi_{\nu_\alpha} \equiv \mu_{\nu_\alpha}/kT$, where

$$L_{\nu_\alpha} \equiv \left(\frac{n_{\nu_\alpha} - n_{\bar{\nu}_\alpha}}{n_\gamma}\right) = \frac{\pi^2}{12\zeta(3)}\left(\frac{T_{\nu_\alpha}}{T_\gamma}\right)^3\left(\xi_{\nu_\alpha} + \frac{\xi_{\nu_\alpha}^3}{\pi^2}\right). \tag{12}$$

Prior to $e^\pm$ annihilation, $T_\nu = T_\gamma$, while post-$e^\pm$ annihilation $(T_\nu/T_\gamma)^3 = 4/11$. Although in principle the asymmetry among the different neutrino flavors may be different, mixing among the three active neutrinos (ν_e, ν_μ, ν_τ) ensures that at BBN, $L_e \approx L_\mu \approx L_\tau$ ($\xi_e \approx \xi_\mu \approx \xi_\tau$)[8]. If L_ν is measured **post**-$e^\pm$ annihilation, as is $\eta_{\rm B}$, then for $\xi_\nu \ll 1$, $L_\nu \approx 3L_{\nu_e}$ and, for $\xi \equiv \xi_e \ll 1$, $L_\nu \approx 0.75\xi$.

Although any neutrino degeneracy ($\xi_{\nu_\alpha} < 0$ as well as > 0) *increases* the energy density in the relativistic neutrinos, resulting in an *effective* $\Delta N_\nu \neq 0$ (see eq. 10), the range of $|\xi|$ of interest to BBN is limited to sufficiently small values that the increase in S due to a non-zero ξ is negligible. However, a small asymmetry between *electron* type neutrinos and antineutrinos ($\xi_e \gtrsim 10^{-2}$; $L \gtrsim 0.007$), while large compared to the baryon asymmetry, can have a significant impact on BBN since the ν_e affect the interconversion of neutrons to protons. A non-zero ξ_e results in different (compared to SBBN) numbers of ν_e and $\bar{\nu}_e$, altering the n/p ratio at BBN, thereby changing the yields (compared to SBBN) of the light nuclides.

Of the light, relic nuclei, the **neutron limited** ^{4}He abundance is most sensitive to a non-zero ξ_e; ^{4}He is a good "leptometer". In concert with the abundances of D, ^{3}He, and ^{7}Li, which are good baryometers, the ^{4}He abundance provides a test of the consistency of the standard model along with constraints on non-standard models. The analytic fits presented below (§2.2) are reasonably accurate for ξ_e in the range, $-0.1 \lesssim \xi_e \lesssim 0.1$, corresponding to a total lepton number limited to $|L| \lesssim 0.07$. While this may seem small, recall that a similar measure of the baryon asymmetry is orders of magnitude smaller: $\eta_{\rm B} \approx 6 \times 10^{-10}$.

2. An Overview of Primordial Nucleosynthesis

The early ($\gtrsim$ 1 ms), hot, dense Universe is filled with radiation (γs, $e^{\pm}$ pairs, νs of all flavors), along with dynamically and numerically insignificant amounts of baryons (nucleons) and dark matter particles. Nuclear and weak interactions are occurring among the neutrons, protons, $e^{\pm}$, and νs (*e.g.*, $n + p \longleftrightarrow D + \gamma$; $p + e^{-} \longleftrightarrow n + \nu_e$) at rates fast compared to the universal expansion rate. At such high temperatures ($T \gtrsim 3$ MeV), in an environment where the nucleon to photon ratio is very small ($\eta_{10} \approx 3 - 10$), the abundances of complex nuclei (D, ^{3}He,^{4}He, ^{7}Li) are tiny in comparison to those of the free nucleons (neutrons and protons). At the same time, the charged-current weak interactions are regulating the neutron to proton ratio, initially keeping it close to its equilibrium value

$$(n/p)_{eq} = e^{-\Delta m/T}, \tag{13}$$

where Δm is the neutron – proton mass (energy) difference. In this context it is worth noting that if there is an *asymmetry* between the numbers of ν_e and $\bar{\nu}_e$ the equilibrium neutron-to-proton ratio is modified to $(n/p)_{eq} = \exp(-\Delta m/T - \mu_e/T) = e^{-\xi_e}(n/p)^0_{eq}$.

As the Universe expands and cools, the lighter protons are favored over the heavier neutrons and the neutron-to-proton ratio decreases, tracking the equilibrium form in eq. 13. But, as the temperature decreases below $T \sim 0.8$ MeV, when the Universe is ~ 1 second old, the weak interactions are too slow to maintain equilibrium and the neutron-to-proton ratio, while continuing to fall, deviates from (*exceeds*) the equilibrium value. Since the n/p ratio depends on the *competition* between the weak interaction rates and the early-Universe expansion rate (as well as on a possible neutrino asymmetry), deviations from the standard model (*e.g.*, $\rho_{\rm R} \to \rho_{\rm R} + \rho_X$ or $\xi_e \neq 0$) will change the relative numbers of neutrons and protons available for building the complex nuclides.

As noted above, while neutrons and protons are interconverting, they are also colliding among themselves creating complex nuclides, *e.g.*, deuterons. However, at early times, when the density and average energy of the CBR photons are very high, the newly formed deuterons find themselves bathed in a background of high-energy gamma rays capable of photodissociating them. Since there are more than a billion CBR photons for every nucleon in the Universe, the deuteron is photodissociated before it can capture a neutron (or a proton, or another deuteron) to build the heavier nuclides. This *bottleneck* to BBN persists until the temperature drops sufficiently below the binding energy of the deuteron, when there are too few photons energetic enough to photodissociate them before they capture nucleons, launching BBN. This transition (smooth, but rapid) occurs after $e^{\pm}$ annihilation, when the Universe is a few minutes old and the temperature has dropped below ~ 80 keV.

Once BBN begins in earnest, neutrons and protons quickly combine to build D, ^{3}H, ^{3}He, and ^{4}He. Since there are no stable mass-5 nuclides, a new bottleneck appears at ^{4}He. Nuclear reactions quickly incorporate all available neutrons into ^{4}He, the most strongly bound of the light nuclides. Jumping the gap at mass-5

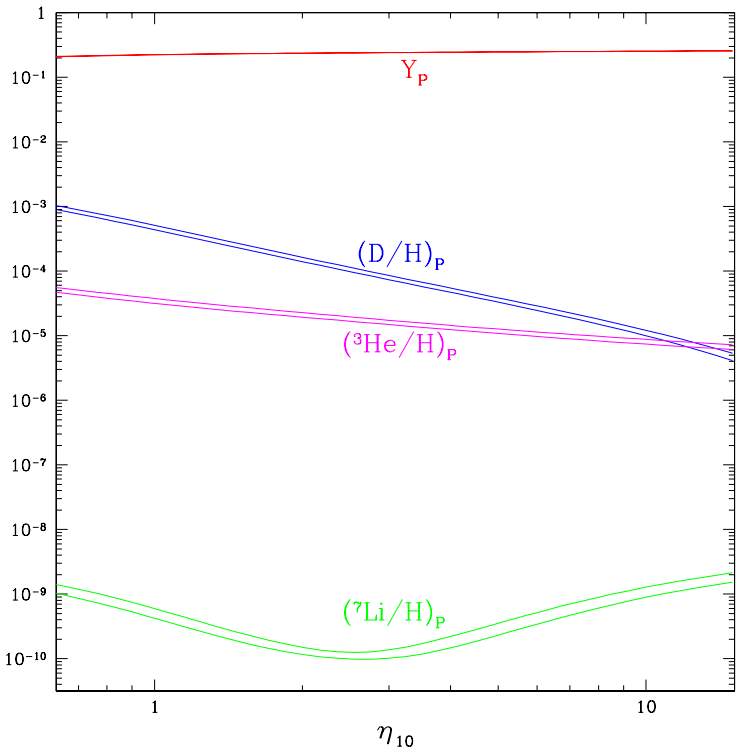

Fig. 1. The SBBN-predicted primordial abundances of D, ^{3}He, ^{7}Li (relative to hydrogen by number), and the ^{4}He mass fraction (Y_P), as functions of the baryon abundance parameter η_{10}. The widths of the bands reflect the uncertainties in the nuclear and weak interaction rates.

requires Coulomb suppressed reactions of ^{4}He with D, or ^{3}H, or ^{3}He, guaranteeing that the abundances of the heavier nuclides are severely depressed below that of ^{4}He (and even of D and ^{3}He), and that the ^{4}He abundance is determined by the neutron abundance when BBN begins. The few reactions that manage to bridge the mass-5 gap lead mainly to mass-7 (^{7}Li or, to ^{7}Be which, later, when the Universe has cooled further, will capture an electron and decay to ^{7}Li); for the range of η_B of interest, the BBN-predicted abundance of ^{6}Li is more than 3 orders of magnitude below that of the more tightly bound ^{7}Li. Finally, there is another gap at mass-8, ensuring that there is no astrophysically significant production of heavier nuclides.

The primordial nuclear reactor is short-lived. As the temperature drops below $T \lesssim 30$ keV, when the Universe is ~ 20 minutes old, Coulomb barriers abruptly suppress all nuclear reactions. Afterwards, until the first stars form, no pre-existing, primordial nuclides are destroyed (except for those like ^{3}H and ^{7}Be that are unstable and decay) and no new nuclides are created. In ~ 1000 seconds BBN has run its

course.

With this as background, the trends of the SBBN-predicted primordial abundances of the light nuclides with baryon abundance shown in Figure 1 can be understood. The reactions burning D and ^{3}He (along with ^{3}H) to ^{4}He are very fast (compared to the universal expansion rate) once the deuterium bottleneck is breached, ensuring that almost all neutrons present at that time are incorporated into ^{4}He. As a result, since ^{4}He production is not *rate limited*, its primordial abundance is very insensitive (only logarithmically) to the baryon abundance. The very slight increase in Y_P with increasing η_B reflects the fact that for a higher baryon abundance BBN begins slightly earlier, when slightly more neutrons are available. The thickness of the Y_P curve in Fig. 1 reflects the very small uncertainty in the BBN prediction; the uncertainty in Y_P ($\sim 0.2\%$; $\sigma_Y \sim 0.0005$) is dominated by the very small error in the weak interaction rates which are normalized by the neutron lifetime ($\tau_n = 885.7 \pm 0.8$ s). The differences among the Y_P predictions from independent BBN codes are typically no larger than $\Delta Y_P \sim 0.0002$.

Nuclear reactions burn D, ^{3}H, and ^{3}He to ^{4}He, the most tightly bound of the light nuclides, at a rate which increases with increasing nucleon density, accounting for the decrease in the abundances of D and ^{3}He (the latter receives a contribution from the β-decay of ^{3}H) with higher values of η_B. The behavior of ^{7}Li is more interesting, reflecting two pathways to mass-7. At the relatively low values of $\eta_{10} \lesssim 3$, mass-7 is largely synthesized as ^{7}Li by ^{3}H(α,γ)^{7}Li reactions. ^{7}Li is easily destroyed in collisions with protons. So, for low nucleon abundance, as η_B increases, destruction is faster than production and ^{7}Li/H *decreases*. In contrast, at relatively high values of $\eta_{10} \gtrsim 3$, mass-7 is largely synthesized as ^{7}Be via ^{3}He(α,γ)^{7}Be reactions. ^{7}Be is more tightly bound than ^{7}Li and, therefore, harder to destroy. As η_B increases at high nucleon abundance, the primordial abundance of ^{7}Be *increases*. Later in the evolution of the Universe, when it is cooler and neutral atoms begin to form, ^{7}Be captures an electron and β-decays to ^{7}Li. These two paths to mass-7 account for the valley shape of the ^{7}Li abundance curve in Fig. 1.

Not shown on Figure 1 are the BBN-predicted relic abundances of ^{6}Li, ^{9}Be, ^{10}B, and ^{11}B. Their production is suppressed by the gap at mass-8. For the same range in η_B, all of them lie offscale, in the range $10^{-20} - 10^{-13}$.

For SBBN the relic abundances of the light nuclides depend on only one free parameter, the nucleon abundance parameter η_B. As Figure 1 reveals, for the "interesting" range (see below) of $4 \lesssim \eta_{10} \lesssim 8$, the ^{4}He mass fraction is expected to be $Y_P \approx 0.25$, with negligible dependence on η_B while D/H and ^{3}He/H decrease from $\approx 10^{-4}$ to $\approx 10^{-5}$, and ^{7}Li/H increases from $\approx 10^{-10}$ to $\approx 10^{-9}$. The light nuclide relic abundances span some nine orders of magnitude, yet if SBBN is correct, one choice of η_B (within the errors) should yield predictions consistent with observations. Before confronting the theory with data, it is useful to consider a few generic examples of BBN in the presence of nonstandard physics and/or cosmology.

2.1. *Nonstandard BBN*

The variety of modifications to the standard models of particle physics and of cosmology is very broad, limited only by the creativity of theorists. Many nonstandard models introduce several, new, free parameters in addition to the baryon abundance parameter $\eta_{\rm B}$. Since there are only four nuclides whose relic abundance is large enough to be astrophysically interesting and, as will be explained below in more detail, only three for which data directly relating to their primordial abundances exist at present (D, ^{4}He, ^{7}Li), nonstandard models with two or more additional parameters may well be unconstrained by BBN. Furthermore, as discussed in the Introduction (see §1.2 and §1.3), there already exist two additional parameters with claims to relevance: the expansion rate parameter S (or, ΔN_ν; see eqs. 8,11) and the lepton asymmetry parameter L (or, ξ; see eq. 12).

The primordial abundance of ^{4}He depends sensitively on the pre- and the post-$e^\pm$ annihilation early universe expansion rate (the Hubble parameter H) and on the magnitude of a $\nu_e - \bar{\nu}_e$ asymmetry because each will affect the n/p ratio at BBN (see, *e.g.*, Steigman, Schramm & Gunn 1977 (SSG)[6]; for recent results see Kneller & Steigman 2004 (KS)[9]). A faster expansion ($S > 1$; $\Delta N_\nu > 0$) leaves less time for neutrons to convert into protons and the higher neutron abundance results in increased production of ^{4}He. For small changes at fixed $\eta_{\rm B}$, $\Delta {\rm Y_P} \approx 0.16(S-1) \approx 0.013\Delta N_\nu$ (KS). Although the relic abundances of D and ^{3}He do depend on the competition between the nuclear reaction rates and the post-$e^\pm$ annihilation expansion rate (faster expansion $\Rightarrow$ less D and ^{3}He destruction $\Rightarrow$ more D and ^{3}He), they are much less sensitive to relatively small deviations from $S = 1$ ($\Delta N_\nu = 0$)[9]. For mass-7 the effect of a nonstandard expansion rate is different at low and high values of $\eta_{\rm B}$. At low baryon abundance ($\eta_{10} \lesssim 3$), a faster expansion leaves less time for ^{7}Li destruction and the relic abundance of mass-7 increases. In contrast, at high baryon abundance ($\eta_{10} \gtrsim 3$), $S > 1$ leaves less time for ^{7}Be production and the relic abundance of mass-7 decreases. As for D and ^{3}He, the quantitative change in the ^{7}Li abundance is small for small deviations from SBBN.

For similar reasons, ${\rm Y_P}$ is sensitive to an asymmetry in the electron neutrinos which, through the charged current weak interactions, help to regulate the n/p ratio. For $\xi_e > 0$, there are more neutrinos than antineutrinos, so that reactions such as $n + \nu_e \longrightarrow p + e^-$, drive down the n/p ratio. For small asymmetry at fixed $\eta_{\rm B}$, KS find $\Delta {\rm Y_P} \approx -0.23\xi_e$. The primordial abundances of D, ^{3}He, and ^{7}Li, while not entirely insensitive to neutrino degeneracy, are much less affected by a nonzero ξ_e than is ^{4}He (*e.g.*, Kang & Steigman 1992[10]).

Each of these nonstandard cases ($S \neq 1$, $\xi \neq 0$) will be considered below. While certainly not exhaustive of the nonstandard models proposed in the literature, they actually have the potential to provide semi-quantitative, if not quantitative, understanding of BBN in a large class of nonstandard models. Note that data constraining the primordial abundances of at least two different relic nuclei (one of which should be ^{4}He) are required to break the degeneracy between the baryon

density and the additional parameter resulting from new physics or cosmology. ^{4}He is a poor baryometer but a very good chronometer and/or, leptometer; D, ^{3}He, ^{7}Li have the potential to be good baryometers.

2.2. *Simple – But Accurate – Fits To The Primordial Abundances*

While BBN involves only a limited number of coupled differential equations, they are non-linear and not easily solved analytically. As a result, detailed comparisons of the theoretical predictions with the inferred relic abundances of the light nuclei requires numerical calculations, which may obscure key relations between abundances and parameters, as well as the underlying physics. In particular, the connection between the cosmological parameter set $\{\eta_{\rm B}, S, \xi_e\}$ and the abundance data set $\{y_{\rm D}, {\rm Y_P}, y_{\rm Li}\}$[b] may be blurred, especially when attempting to formulate a quantitative understanding of how the latter constrains the former. However, it is clear from Figure 1 that the relic, light nuclide abundances are smoothly varying, monotonic functions of $\eta_{\rm B}$ over a limited but substantial range. While the BBN-predicted primordial abundances are certainly *not* linearly related to the baryon density (nor to the other parameters S and ξ_e), over the restricted ranges identified above, KS[9] found linear fits to the predicted abundances (or, to powers of them) which work very well indeed. Introducing them here enables and simplifies the comparison of theory with data (below) and permits a quick, reasonably accurate, back of the envelope, identification of the successes of and challenges to BBN.

For the adopted range of $\eta_{\rm B}$, $y_{\rm D} = y_{\rm D}(\eta_{\rm B})$ is well fit by a power law,

$$y_{\rm D}^{FIT} \equiv 46.5\eta_{10}^{-1.6}. \tag{14}$$

While the true $y_{\rm D} - \eta_{\rm B}$ relation is not precisely a power law, this fit (for $4 \lesssim \eta_{10} \lesssim 8$) is accurate (compared to a numerical calculation) to better than 1%, three times smaller than the $\sim 3\%$ BBN uncertainty estimated by Burles, Nollett, Turner 2001 (BNT)[11]; this fit and the numerical calculation agree with the BNT result to 2% or better over the adopted range in $\eta_{\rm B}$. Note that since different BBN codes are largely independent and often use somewhat different nuclear reaction data sets, the *differences* among their predicted abundances may provide estimates of the overall uncertainties. It is convenient to introduce a "deuterium baryon density parameter" $\eta_{\rm D}$, the value of η_{10} corresponding to an observationally determined primordial D abundance.

$$\eta_{\rm D} \equiv (\frac{46.5(1 \pm 0.03)}{y_{\rm D}})^{1/1.6}. \tag{15}$$

Generalizing this to include the two other parameters, KS find

$$\eta_{\rm D} = \eta_{10} - 6(S-1) + \frac{5\xi_e}{4}. \tag{16}$$

[b]${\rm Y_P}$ is the ^{4}He *mass fraction* while the other abundances are measured by *number* compared to hydrogen. For numerical convenience, $y_{\rm D} \equiv 10^5({\rm D/H})$ and $y_{\rm Li} \equiv 10^{10}({\rm Li/H})$.

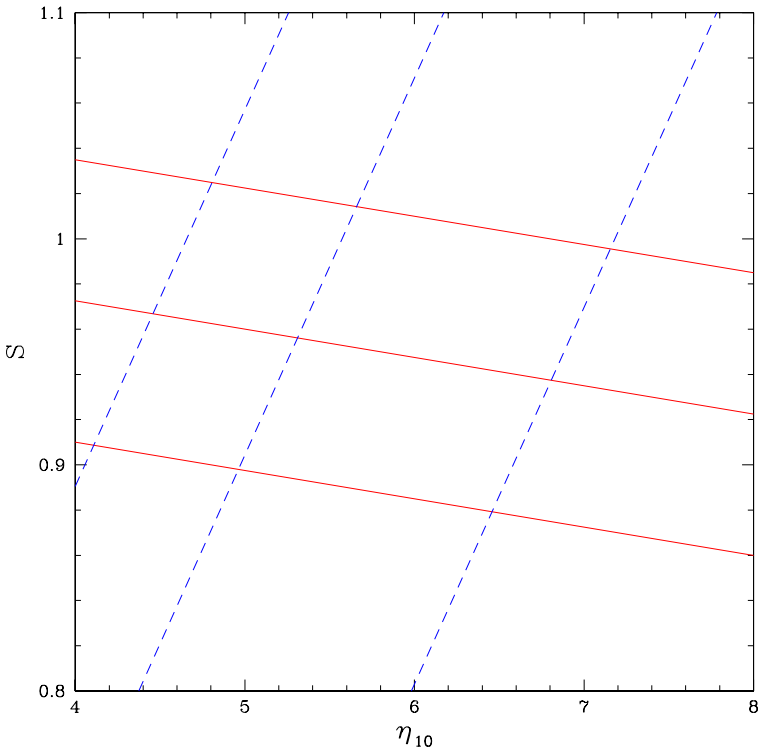

Fig. 2. Isoabundance curves for Deuterium (dashed lines) and Helium-4 (solid lines) in the expansion rate factor (S) – baryon abundance (η_{10}) plane. The ^{4}He curves, from bottom to top, are for $Y_P = 0.23, 0.24, 0.25$. The D curves, from left to right, are for $y_D = 4.0, 3.0, 2.0$.

This fit works quite well for $2 \lesssim y_D \lesssim 4$, corresponding to $5 \lesssim \eta_D \lesssim 7$. In Figure 2 the deuterium isoabundance curves are shown in the $S - \eta_{10}$ plane, while Figure 3 shows the same isoabundance contours in the $\xi_e - \eta_{10}$ plane. It is clear from Figures 2 and 3 that D is a sensitive *baryometer* since, for these ranges of S and ξ_e, $\eta_D \approx \eta_{10}$.

Next, consider ^{4}He. While over a much larger range in η_{10}, Y_P varies nearly *logarithmically* with the baryon density parameter, a *linear* fit to the Y_P versus η_{10} relation is actually remarkably accurate over the restricted range considered here.

$$Y_P^{FIT} \equiv 0.2384 + 0.0016\eta_{10} = 0.2384 + \eta_{10}/625. \tag{17}$$

Over the same range in η_{10} this fit agrees with the numerical calculation and with the BNT[11] predictions for Y_P to within 0.0002 ($\lesssim 0.1\%$), or better. Any differences between this fit and independent, numerical calculations are smaller (much smaller) than current estimates of the errors in the observationally inferred primordial value

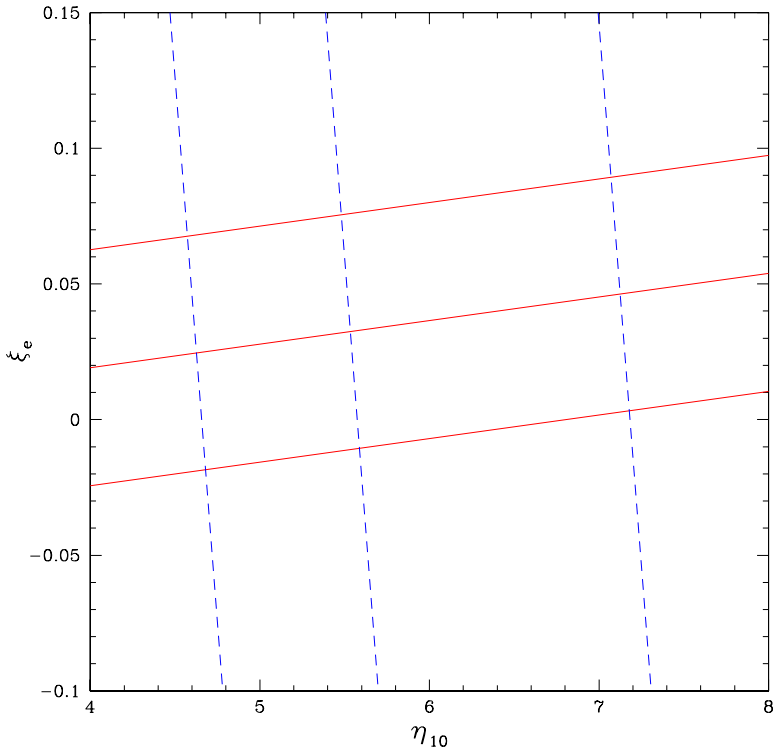

Fig. 3. As in Figure 2, in the neutrino asymmetry (ξ_e) – baryon abundance (η_{10}) plane. The ^{4}He curves, from bottom to top, are for $Y_P = 0.25, 0.24, 0.23$. The D curves, from left to right, are for $y_D = 4.0, 3.0, 2.0$.

of Y_P. The following linear fits, including the total error estimate, to the $Y_P - S$ and $Y_P - \xi_e$ relations from KS work very well over the adopted parameter ranges (see Figures 2 & 3).

$$Y_P^{FIT} \equiv 0.2384 \pm 0.0006 + 0.0016\eta_{10} + 0.16(S-1) - 0.23\xi_e. \quad (18)$$

As an aside, the dependence of the ^{4}He mass fraction on the neutron lifetime (τ_n) can be included in eq. 18 by adding a term $0.0002(\tau_n - 887.5)$, where τ_n is in seconds. A very recent, new measurement of τ_n by Serebrov *et al.*[12] suggests that the currently accepted value ($\tau_n = 887.5$ s) should be reduced by 7.2 s. If confirmed, this would lead to a slightly smaller BBN-predicted ^{4}He abundance: $\Delta Y_P = -0.0014$. The corresponding shift in the ^{4}He inferred baryon density parameter is negligible compared to its range of uncertainty ($\Delta\eta_B/\eta_B = -0.14$), as is that for the shift in the upper bound to N_ν ($\Delta N_\nu^{max} = +0.11$). These corrections are ignored here.

In analogy with the deuterium baryon density parameter introduced above, it

is convenient to introduce $\eta_{\rm He}$, defined by

$$\eta_{\rm He} \equiv 625({\rm Y_P} - 0.2384 \pm 0.0006), \tag{19}$$

so that

$$\eta_{\rm He} = \eta_{10} + 100(S-1) - \frac{575\xi_e}{4}. \tag{20}$$

For SBBN ($S = 1$ & $\xi_e = 0$), $\eta_{\rm He}$ is the value of η_{10} corresponding to the adopted value of $\rm Y_P$. Once $\rm Y_P$ is chosen, the resulting value of $\eta_{\rm He}$ provides a *linear* constraint on the combination of η_{10}, S, and ξ_e in eq. 20. This fit works well[9] for $0.23 \lesssim {\rm Y_P} \lesssim 0.25$, corresponding to $-5 \lesssim \eta_{\rm He} \lesssim 7$. As Figures 2 & 3 reveal, ^{4}He is an excellent chronometer and/or leptometer, since the $\rm Y_P$ isoabundance curves are nearly horizontal (and very nearly orthogonal to the deuterium isoabundance curves).

As with D, the ^{7}Li abundance[c] is well described by a power law in η_{10} over the range in baryon abundance explored here: $y_{\rm Li} \equiv 10^{10}({\rm Li/H}) \propto \eta_{10}^2$. The following KS fit agrees with the BBN predictions to better than 3% over the adopted range in η_{10},

$$y_{\rm Li}^{FIT} \equiv \frac{\eta_{10}^2}{8.5}. \tag{21}$$

While this fit predicts slightly smaller lithium abundances compared to those of BNT[11], the differences are at the 5-8% level, small compared to the BNT uncertainty estimates as well as those of Hata *et al.* (1995)[13] ($\sim 10 - 20\%$).

In analogy with $\eta_{\rm D}$ and $\eta_{\rm He}$ defined above, the lithium baryon abundance parameter $\eta_{\rm Li}$ (allowing for a 10% overall uncertainty) is defined by

$$\eta_{\rm Li} \equiv (8.5(1 \pm 0.1)y_{\rm Li})^{1/2}. \tag{22}$$

The simple, linear relation for $\eta_{\rm Li}$ as a function of η_{10}, S, ξ_e, which KS find fits reasonably well over the adopted parameter ranges is,

$$\eta_{\rm Li} = \eta_{10} - 3(S-1) - \frac{7\xi_e}{4}. \tag{23}$$

This fit works well for $3 \lesssim y_{\rm Li} \lesssim 5$, corresponding to $5 \lesssim \eta_{\rm Li} \lesssim 7$, but it breaks down for $y_{\rm Li} \lesssim 2$ ($\eta_{\rm Li} \lesssim 4$); see Fig. 1. As is the case for deuterium, lithium can be an excellent baryometer since, for the restricted ranges of S and ξ_e under consideration here, $\eta_{\rm Li} \approx \eta_{10}$.

Finally, it may be of interest to note that for ^{3}He the power law $y_3 - \eta_{\rm B}$ relation, where $y_3 \equiv 10^5(^3{\rm He/H})$, which is reasonably accurate for $4 \lesssim \eta_{10} \lesssim 8$ is

$$y_3 = 3.1(1 \pm 0.03)\eta_{10}^{-0.6}. \tag{24}$$

The difficulty of using current observational data, limited to chemically evolved regions of the Galaxy, to infer the primordial abundance of ^{3}He, along with the

[c]It is common in the astronomical literature to present the lithium abundance logarithmically: [Li] $\equiv 12 + \log({\rm Li/H}) = 2 + \log({\rm y_{Li}})$.

relatively weak dependence of y_3 on η_{10}, limits the utility of this nuclide as a baryometer[14]. ^{3}He can, however, be used as a test of BBN consistency.

2.3. *SBBN-Predicted Primordial Abundances*

Before discussing the current status of the observationally determined abundances (and their uncertainties) of the light nuclides, it is interesting to *assume* SBBN and, for the one free parameter, $\eta_{\rm B}$, use the value inferred from non-BBN data such as the CBR (WMAP) and Large Scale Structure (LSS)[2] to predict the relic abundances.

From WMAP alone, Spergel *et al.* 2003[2] derive $\eta_{10} = 6.3 \pm 0.3$. Using the fits from §2.2, with $S = 1$ and $\xi_e = 1$, the SBBN-predicted relic abundances are: $y_{\rm D} = 2.45 \pm 0.20$; $y_3 = 1.03 \pm 0.04$; $\rm Y_P = 0.2485 \pm 0.0008$; $y_{\rm Li} = 4.67 \pm 0.64$ ($[{\rm Li}]_{\rm P} = 2.67 \pm 0.06$).

When Spergel *et al.* 2003[2] combine the WMAP CBR data with those from Large Scale Structure, they derive a consistent, but slightly smaller (slightly more precise) baryon abundance parameter $\eta_{10} = 6.14 \pm 0.25$. For this choice the SBBN-predicted relic abundances are: $y_{\rm D} = 2.56 \pm 0.18$; $y_3 = 1.04 \pm 0.04$; $\rm Y_P = 0.2482 \pm 0.0007$; $y_{\rm Li} = 4.44 \pm 0.57$ ($[{\rm Li}]_{\rm P} = 2.65^{+0.05}_{-0.06}$).

3. Observationally Inferred Primordial Abundances

3.1. *The Primordial Deuterium Abundance*

Deuterium is the baryometer of choice since its post-BBN evolution is simple (and monotonic!) and its BBN-predicted relic abundance depends sensitively on the baryon abundance ($y_{\rm D} \propto \eta_{\rm B}^{-1.6}$). As the most weakly bound of the light nuclides, any deuterium cycled through stars is burned to ^{3}He and beyond during the pre-main sequence, convective (fully mixed) evolutionary stage[15]. Thus, deuterium observed anywhere, anytime, should provide a *lower* bound to the primordial D abundance. For "young" systems at high redshift and/or with very low metallicity, which have experienced very limited stellar evolution, the observed D abundance should be close to the primordial value. Thus, although there are observations of deuterium in the solar system and the interstellar medium (ISM) of the Galaxy which provide interesting *lower* bounds to the primordial abundance, it is the observations of relic D in a few (too few!), high redshift, low metallicity, QSO absorption line systems (QSOALS) which are of most value in enabling estimates of its primordial abundance.

In contrast to the great asset of the simple post-BBN evolution, the identical absorption spectra of D I and H I (modulo the velocity/wavelength shift resulting from the heavier reduced mass of the deuterium atom) is a severe liability, limiting drastically the number of useful targets in the vast Lyman-alpha forest of QSO absorption spectra (see Kirkman *et al.*[16] for further discussion). As a result, it is essential to choose target QSOALS whose velocity structure is "simple" since a

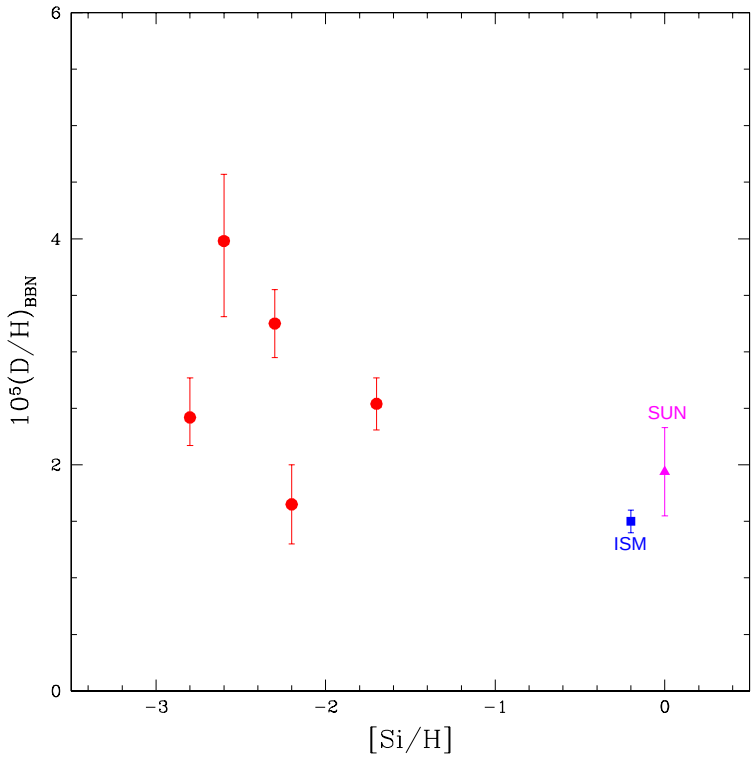

Fig. 4. The observationally inferred primordial deuterium abundances (the ratio of D to H by number) versus a logarithmic measure of the metallicity, relative to solar ([Si/H]), for five high redshift, low metallicity QSOALS (filled circles) through 2003. The error bars are the quoted 1σ uncertainties. Also shown for comparison are the D/H ratios inferred from observations of the local interstellar medium (ISM; filled square) and that for the pre-solar nebula (Sun; filled triangle).

low column density H I absorber, shifted by ~ 81 km/s with respect to the main H I absorber (an "interloper") could masquerade as D I absorption[17]. If this degeneracy is not recognized, a D/H ratio which is too high could be inferred. Since there are many more low-column density absorbers than those with high H I column densities, absorption systems with somewhat lower H I column density (*e.g.*, Lyman-limit systems: LLS) may be more susceptible to this contamination than the higher H I column density absorbers (*e.g.*, damped Lyα absorbers: DLA). While the DLA do have many advantages over the LLS, a precise determination of the H I column density utilizing the damping wings of the H I absorption requires an accurate placement of the continuum, which could be compromised by H I interlopers. This might lead to errors in the H I column density. These complications are real and the path to primordial D using QSOALS has not been straightforward, with some abundance claims having had to be withdrawn or revised. Through 2003 there were

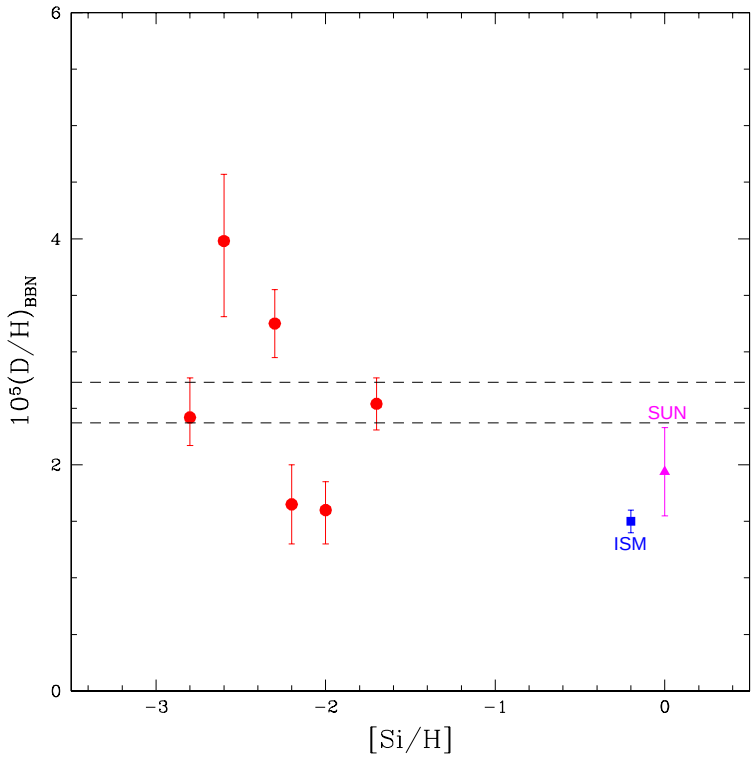

Fig. 5. Figure 4 updated to 2004 to include the one new deuterium abundance determination[18] for a high redshift, low metallicity QSOALS. The dashed lines show the SBBN-predicted 1σ band for the WMAP baryon abundance.

only five "simple" QSOALS with deuterium detections leading to reasonably robust abundance determinations[16] (and references therein); these are shown in Figure 4 along with the corresponding solar system and ISM D abundances. It is clear from Figure 4, that there is significant dispersion among the derived D abundances at low metallicity which, so far, masks the anticipated primordial deuterium plateau, suggesting that systematic (or random) errors, whose magnitudes are hard to estimate, may have contaminated the determinations of the D I and/or H I column densities.

It might be hoped that as more data are acquired, the excessive dispersion among the deuterium abundances seen in Fig. 4 would decrease leading to a better defined deuterium plateau. Be careful what you wish for! In 2004, Crighton *et al.*[18] identified deuterium absorption in another high redshift, low metallicity QSOALS and derived its abundance. The updated version of Fig. 4 is shown in Fig. 5. Now, the dispersion is **larger**! The low value of the Crighton *et al.*[18] D abundance,

similar to that in the more highly evolved ISM and the pre-solar nebula, is puzzling. D. Tytler (private communication) and colleagues have data (unpublished) for the same QSOALS and they find acceptable fits with lower H I column densities and no visible D I; perhaps this system is contaminated by an interloper[17]. The two low D/H ratios, if not affected by random or systematic errors, may be artifacts of a small statistical sample or, they may have resulted from "young" regions in which some of the relic deuterium has been destroyed or depleted onto dust[19]. These suggestions pose challenges since any cycling of gas through stars should have led to an *increase* in the heavy element abundances (these QSOALS are metal poor) and, at low metallicity the amount of dust is expected to be small.

For the Spergel *et al.*[2] baryon abundance of $\eta_{10} = 6.14 \pm 0.25$, the SBBN-predicted deuterium abundance is $y_{\rm D} = 2.6 \pm 0.2$. As may be seen in Fig. 5, the current data exhibit the Goldilocks effect: two D/H ratios are "too small", two are "too large", and two are "just right". Nonetheless, it is clear that the sparse data currently available are in very good agreement with the SBBN prediction. If the weighted mean of D/H for the six QSOALS is adopted, but the dispersion in the mean is used in place of the error in the mean, $y_{\rm D} = 2.4 \pm 0.4$, corresponding to an SBBN-predicted baryon abundance of $\eta_{10} = 6.4 \pm 0.6$, in excellent agreement with the WMAP value. Were it not for the excessive dispersion among the extant deuterium abundance determinations, the precision of the baryon abundance determined from SBBN would be considerably enhanced. For example, if the formal error in the mean is used, $\eta_{10} = 6.4 \pm 0.2$ is the deuterium-based, SBBN prediction, very close to that for the baryon abundance derived from the CBR alone[2] ($\eta_{10}^{\rm WMAP} = 6.3 \pm 0.3$). More data is crucial to deuterium fulfilling its potential.

3.2. *The Primordial Helium-3 Abundance*

The post-BBN evolution of ^{3}He, involving competition among stellar production, destruction, and survival, is considerably more complex and model dependent than that of D. Interstellar ^{3}He incorporated into stars is burned to ^{4}He (and beyond) in the hotter interiors, but it is preserved in the cooler, outer layers. Furthermore, while hydrogen burning in cooler, low-mass stars is a net producer of ^{3}He[20], it is unclear how much of this newly synthesized ^{3}He is returned to the interstellar medium and how much of it is consumed in post-main sequence evolution (*e.g.*, Sackmann & Boothroyd[21]). For years it had been anticipated that net stellar production would prevail in this competition, so that the ^{3}He abundance would increase with time (and with metallicity)[22].

Observations of ^{3}He, are restricted to the solar system and the Galaxy. Since for the latter there is a clear gradient of metallicity with location, a gradient in ^{3}He abundance was also expected. However, as is clear from Figures 6 & 7, the data[23,24] reveal no statistically significant correlation between the ^{3}He abundance and metallicity or location in the Galaxy, suggesting a very delicate balance between net production and net destruction of ^{3}He. For a recent review of the current status

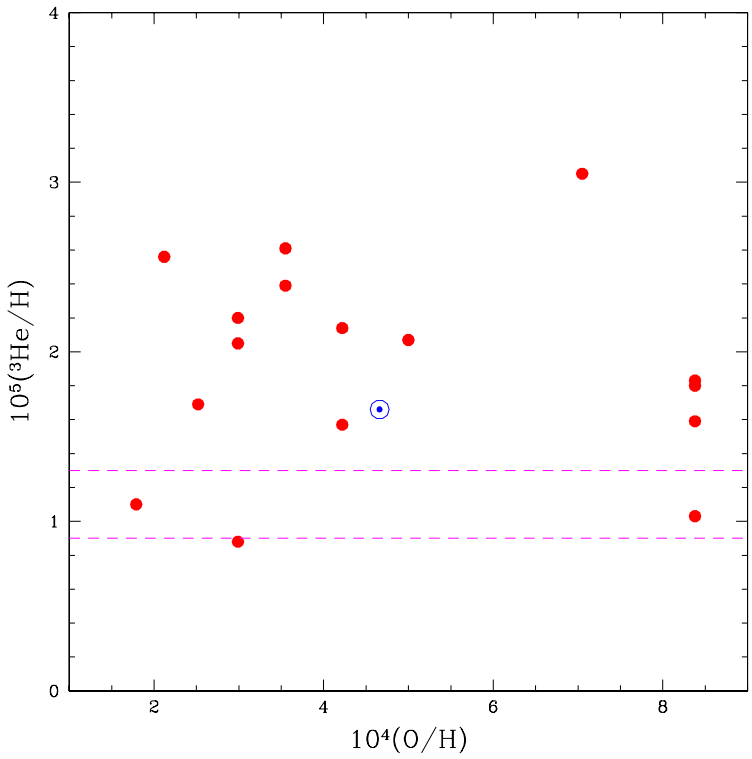

Fig. 6. The ^{3}He abundance determinations (by number relative to H) in the ISM of the Galaxy (from BRB[24]) as a function of the corresponding oxygen abundances. The solar symbol indicates the ^{3}He abundance for the pre-solar nebula. The dashed lines show the 1σ band adopted by BRB.

of ^{3}He evolution, see Romano *et al.*[25].

While the absence of a gradient suggests the *mean* ("plateau") ^{3}He abundance in the Galaxy ($y_3 \approx 1.9 \pm 0.6$) might provide a good estimate of the primordial abundance, Bania, Rood & Balser (BRB)[24] prefer to adopt as an upper limit to the primordial abundance, the ^{3}He abundance measured in the most distant (from the Galactic center), most metal poor, Galactic H II region, $y_3 \lesssim 1.1 \pm 0.2$; see Figs. 6 & 7. This choice is in excellent agreement with the SBBN/WMAP predicted abundance of $y_3 = 1.04 \pm 0.04$ (see §2.2). While both D and ^{3}He are consistent with the SBBN predictions, ^{3}He is a less sensitive baryometer than is D since $(\mathrm{D/H})_{\rm BBN} \propto \eta_{\rm B}^{-1.6}$, while $(^3\mathrm{He/H})_{\rm BBN} \propto \eta_{\rm B}^{-0.6}$. For example, if $y_3 = 1.1 \pm 0.2$ is adopted for the ^{3}He primordial abundance, $\eta_{10}(^3\mathrm{He}) = 6.0 \pm 1.7$. While the central value of the ^{3}He-inferred baryon density parameter is in nearly perfect agreement with the WMAP value[2], the allowed range of $\eta_{\rm B}$ is far too large to be very useful. Still, ^{3}He can provide a valuable BBN consistency check.

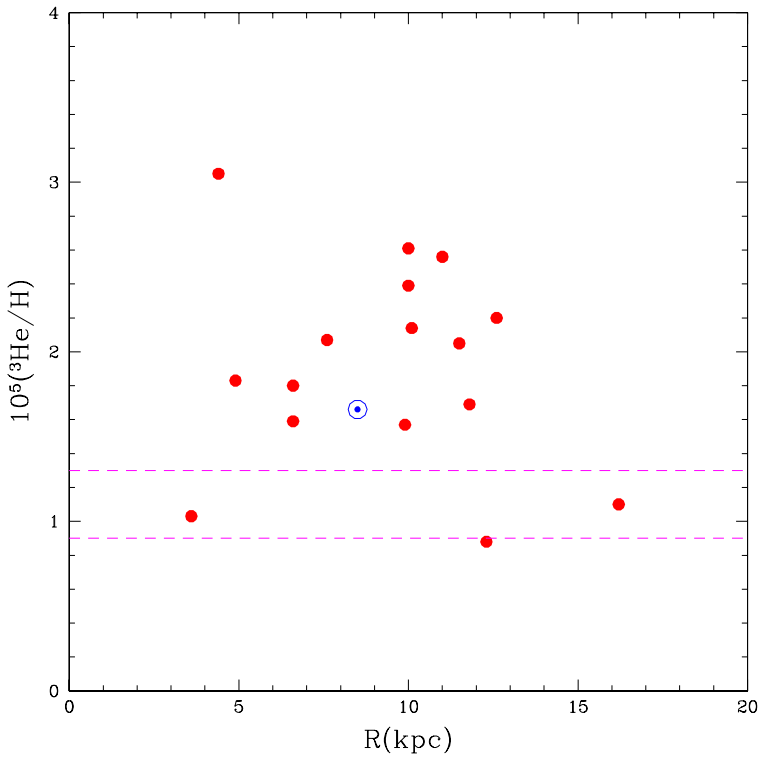

Fig. 7. As in Figure 6 but, for the ^{3}He abundances as a function of distance from the center of the Galaxy.

3.3. *The Primordial Helium-4 Abundance*

The post-BBN evolution of ^{4}He is quite simple. As gas cycles through generations of stars, hydrogen is burned to helium-4 (and beyond), increasing the ^{4}He abundance above its primordial value. The ^{4}He mass fraction in the Universe at the present epoch, Y_0, has received a significant contribution from post-BBN, stellar nucleosynthesis, so that $Y_0 > Y_P$. However, since the "metals" such as oxygen are produced by short-lived, massive stars and ^{4}He is synthesized (to a greater or lesser extent) by all stars, at very low metallicity the increase in Y should lag that in *e.g.*, O/H so that as O/H $\rightarrow 0$, Y $\rightarrow Y_P$. As is the case for deuterium and lithium, a ^{4}He "plateau" is expected at sufficiently low metallicity. Therefore, although ^{4}He is observed in the Sun and in Galactic H II regions, the key data for inferring its primordial abundance are provided by observations of helium and hydrogen emission (recombination) lines from low-metallicity, extragalactic H II regions. The present inventory of such regions studied for their helium content exceeds 80 (see Izotov & Thuan (IT)[26]). Since with such a large data set even modest observational errors

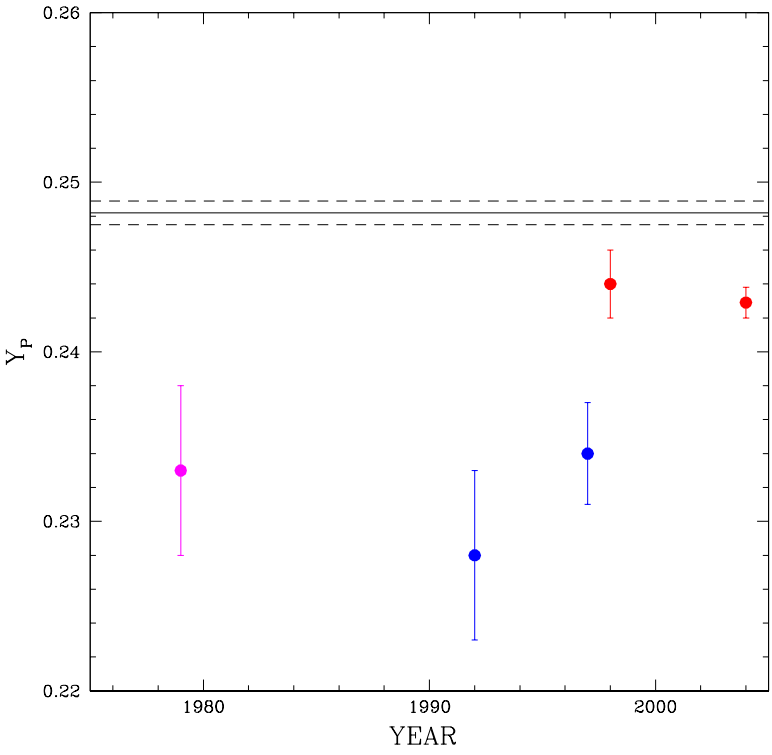

Fig. 8. The observationally inferred primordial ^{4}He mass fractions from 1978 until 2004. The error bars are the quoted 1σ uncertainties. Also shown is the SBBN-predicted relic abundance (solid line) for the WMAP baryon abundance, along with the 1σ uncertainty (dashed lines) of the SBBN prediction.

for the individual H II regions can lead to an inferred primordial abundance whose formal *statistical* uncertainty may be quite small, special care must be taken to include hitherto ignored or unaccounted for *systematic* corrections and/or errors. It is the general consensus that the present uncertainty in Y_P is dominated by the latter, rather than by the former errors. Indeed, many of the potential pitfalls were identified by Davidson & Kinman[27] in a prescient, 1985 paper. In the abstract they say, "The most often quoted estimates of the primordial helium abundance are optimistic in the sense that quoted uncertainties usually do not include some potentially serious systematic errors."

To provide a context for the discussion of the most recent data and analyses, Figure 8 offers a compilation of the history of Y_P determinations[26,28] derived using data from low metallicity, extragalactic H II regions. Notice that all of these estimates, taken at face value, fall below the SBBN/WMAP predicted primordial

abundance by at least 2σ, reemphasizing the importance of accounting for systematic uncertainties. With this in mind, we turn to recent reanalyses[29,30] of the IT data[26], supplemented by key observations of a local, higher metallicity H II region[30].

Prior and subsequent to the Davidson & Kinman paper[27] astronomers have generally been aware of the important sources of potential systematic errors associated with using recombination line data to infer the helium abundance. However, attempts to account for them have often been unsystematic or, entirely absent. The current conventional wisdom that the accuracy of the data demands their inclusion has led to some attempts to account for a few of them or, for combinations of a few of them[26,29,30,31,32]. The Olive & Skillman (OS)[29] analysis of the IT data is the most systematic to date. Following criteria outlined in their 2001 paper[29], OS found they were able to apply their analysis to only 7 of the 82 IT H II regions. This tiny data set, combined with its limited range in metallicity (oxygen abundance), severely limits the statistical significance of any conclusions OS can extract from it. In Figure 9 are shown the *differences* between the OS-inferred and the IT-inferred helium abundances. For these seven H II regions there is no evidence that $\Delta Y \equiv Y^{OS} - Y^{IT}$ is correlated with metallicity. The weighted mean offset along with the error in the mean are $\Delta Y = 0.0029 \pm 0.0032$ (the *average* offset and the *average* error are $\Delta Y = 0.0009 \pm 0.0095$), consistent with zero at 1σ.

If the weighted mean offset is applied to the IT-derived primordial abundance of $Y_P^{IT} = 0.2443 \pm 0.0015$, the "corrected" primordial value becomes

$$Y_P^{OS} \equiv Y_P^{IT} + \Delta Y = 0.2472 \pm 0.0035, \tag{25}$$

leading to a 2σ *upper* bound on the primordial abundance of $Y_P^{OS} \leq 0.254$. In contrast, OS prefer to fit these seven data points to a *linear* Y versus O/H relation and, from it, derive the primordial abundance. Their IT-revised abundances, along with, for comparison, that from their reanalysis of the Peimbert *et al.*[30] data for an H II region in the SMC (to be discussed next), are shown in Figure 10. It is not surprising that for only seven data points, each with larger errors than those adopted by IT, spanning such a narrow range in metallicity, their linear fit, $Y_7^{OS} = 0.2495 \pm 0.0092 + (54 \pm 187)(O/H)$, is **not** statistically significant. Indeed, it is **not** preferred over the simple weighted mean of the seven helium abundances (0.252 ± 0.003), since the χ^2 per degree of freedom is actually *higher* for the linear fit. In fact, there is no statistically significant correlation between Y and O/H for the IT-derived abundances for these seven H II regions either. As valuable as is their reanalysis of the IT data, the OS conclusion that $Y_P = 0.249 \pm 0.009$ is not supported by the sparse data set they used[d]. Unless and until an analysis is performed of a much larger data set, with a longer metallicity baseline, the estimate in eq. 25, and its corresponding 2σ upper bound, may provide a good starting point at present for an approach to the primordial abundance of ^{4}He.

[d]Note that OS used the corresponding 1σ upper bound of 0.258 for the upper bound to their "favored" primordial abundance range.

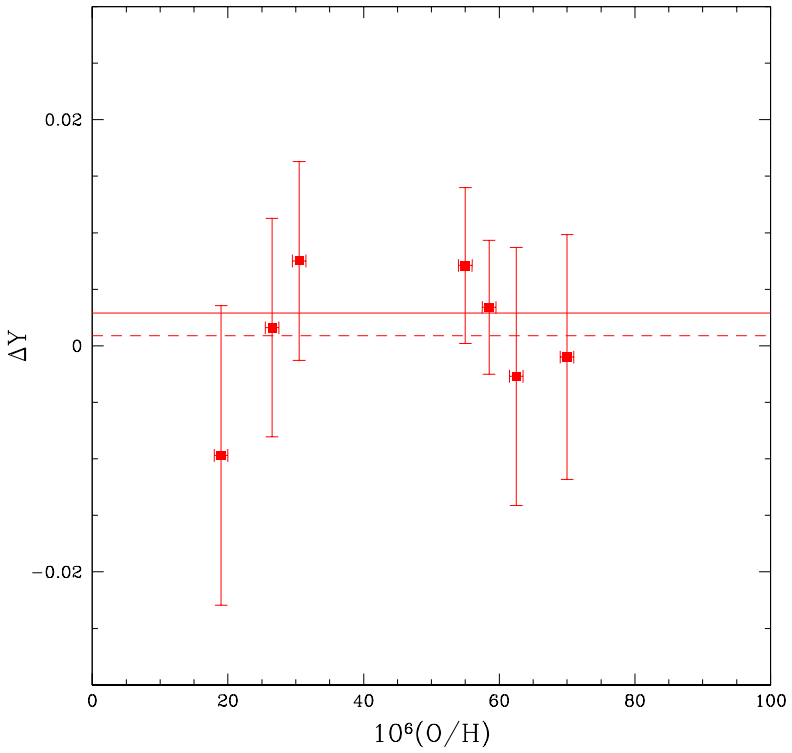

Fig. 9. The ***differences*** between the OS and IT ^{4}He abundances, $\Delta Y \equiv Y^{OS} - Y^{IT}$ for the OS-selected IT H II regions versus the corresponding oxygen abundances. The solid line is the weighted mean of the helium mass fraction differences, while the dashed line shows the unweighted *average* of the differences.

Another correction, not directly constrained by the analysis of OS, is related to the inhomogeneous nature of H II regions. Unlike classical, textbook, homogeneous, Strömgren spheres, real H II regions are filamentary and inhomogeneous, with variations in electron density and temperature likely produced by shocks and winds from pockets of hot, young stars. Esteban and Peimbert[33] have noted that temperature fluctuations can have a direct effect on the helium abundance derived from recombination lines. This effect was investigated theoretically using models of H II regions[31], but more directly by Peimbert *et al.*[30] using data from a nearby, spatially resolved, H II region in the Small Magellanic Cloud (SMC), along with their reanalyses of four H II regions selected from IT. While the SMC H II region formed out of chemically evolved gas and, therefore, cannot be used by itself to derive primordial abundances, the spatial resolution it offers permits a direct investigation of many potential systematic effects. In particular, since recombination lines are used, the observations are blind to any neutral helium or hydrogen. Estimates of the "ion-

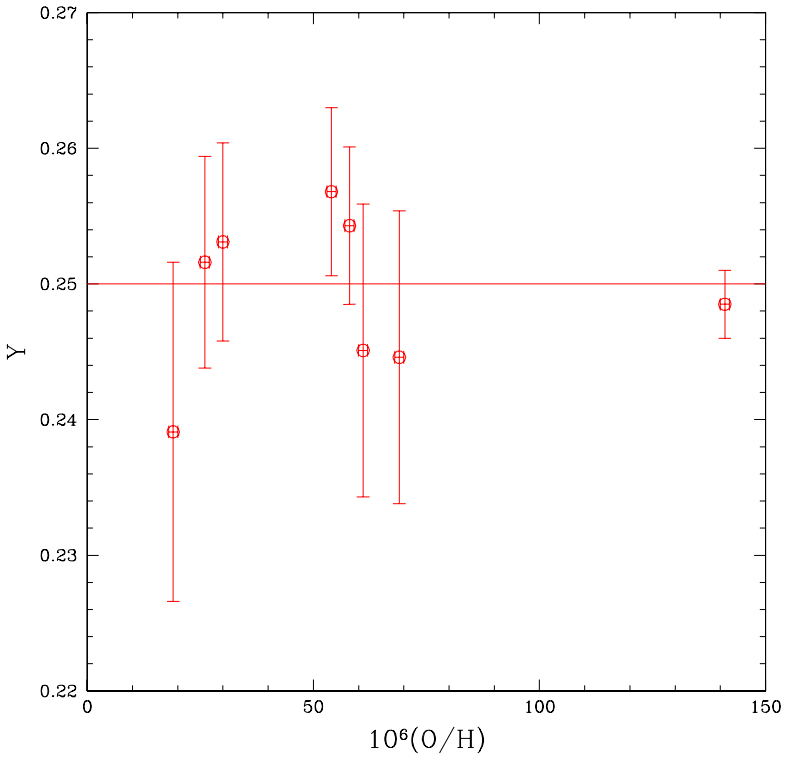

Fig. 10. The OS-revised ^{4}He versus oxygen abundances for the seven IT H II regions and the SMC H II region from PPR. The solid line is the weighted mean of the helium abundances for all eight of the H II regions reanalyzed by OS.

ization correction factor" (*icf*), while model dependent, are large[32]. For example, using models of H II regions ionized by distributions of stars of different masses and ages and comparing to the IT (1998) data, Gruenwald *et al.*[32] concluded that IT *overestimated* the primordial ^{4}He abundance by $\Delta Y^{GSV}(icf) \approx 0.006 \pm 0.002$; Sauer & Jedamzik[32] find a similar, even larger, correction. If this correction is applied to the OS-revised, IT primordial abundance in eq. 25, the new, *icf*-corrected value is

$$Y_P^{GSV}(icf) \equiv Y_P^{OS} - \Delta Y^{GSV}(icf) = 0.241 \pm 0.004. \quad (26)$$

In addition to the subset of 7 of the 82 IT H II regions which meet their criteria, OS also reanalyzed the Peimbert *et al.* data[30] for the SMC H II region. This OS-revised data point is shown in Figure 10 at the highest oxygen abundance. Notice that the eight data points plotted in Fig. 10 show no evidence of the expected *increase* of Y with metallicity[e]; this is likely due to the small sample size. The

[e]Absence of evidence is NOT evidence of absence.

weighted mean ^{4}He abundance for these eight H II regions is $Y_8^{OS} = 0.250 \pm 0.002$, corresponding to a 2σ upper bound of $Y_P \leq 0.254$. Coincidentally, this is the same 2σ upper bound as that found from the mean of the seven IT H II regions (see eq. 25) and, also, the 2σ upper bound from the OS-reanalyzed SMC H II region alone. If the ionization corrections from Gruenwald *et al.*[32] are applied to each of these eight H II regions, it is found that the mean $\Delta Y(icf)_8 = -0.002 \pm 0.002$, so that including this correction, while accounting for the increased error, leaves the 2σ upper bound of $Y_P \leq 0.254$ unchanged.

The lesson from the discussion above is that while recent attempts to determine the primordial abundance of ^{4}He may have achieved high *precision*, their *accuracy* remains in question. The latter is limited by our understanding of and our ability to account for systematic errors and biases, not by the statistical uncertainties. The good news is that carefully organized, detailed studies of only a few ($\sim$ a dozen?) low metallicity, extragalactic H II regions may go a long way towards an accurate determination of Y_P. The bad news is that many astronomers and telescope allocation committee members are unaware that this is an interesting and important problem, worth their effort and telescope time. At present then, the best that can be done is to adopt a defensible value for Y_P and, especially, its uncertainty. To this end, in the following the estimate in eq. 26 is chosen: $Y_P = 0.241 \pm 0.004$. While the central value of Y_P is low, it is within 2σ ($\sim 1.75\sigma$) of the SBBN/WMAP expected central value of $Y_P = 0.248$ (see §2.2). Note that the *extrapolation* of the linear fit of the {Y, O/H} data from the lowest metallicity (O/H $\approx 2 \times 10^{-5}$) to zero metallicity (Y_P) corresponds to $\Delta Y \approx 0.0009$, well within the uncertainties of Y_P.

In setting contraints on new physics, an upper bound to Y_P is required. A robust upper bound suggested by the above discussion is $Y_P \leq 0.254$. As an example, the SBBN/WMAP lower bound (at $\sim 2\sigma$) to Y_P is 0.247, so that $\Delta Y_P < 0.007$. This corresponds to the robust upper bounds $S < 1.04$ and $N_\nu < 3.5$, eliminating (just barely) even one, new, light scalar, and bounding the lepton asymmetry from below: $\xi_e > -0.03$.

3.4. *The Primordial Lithium-7 Abundance*

In the post-BBN universe ^{7}Li, along with ^{6}Li, ^{9}Be, ^{10}B, and ^{11}B, is produced in the Galaxy by cosmic ray spallation/fusion reactions. Furthermore, observations of super-lithium rich red giants provide evidence that (at least some) stars are net producers of lithium. Therefore, even though lithium is easily destroyed in the hot interiors of stars, theoretical expectations supported by the observational data shown in Figure 11 suggest that while lithium may have been depleted in many stars, the overall trend is that its abundance has increased with time. Therefore, in order to probe the BBN yield of ^{7}Li, it is necessary to restrict attention to the oldest, most metal-poor halo stars in the Galaxy (the "Spite Plateau") seen at low metallicity in Fig. 11. Using a selected set of the lowest metallicity halo stars, Ryan *et al.*[34] claim evidence for a 0.3 dex increase in the lithium abundance ([Li] $\equiv$

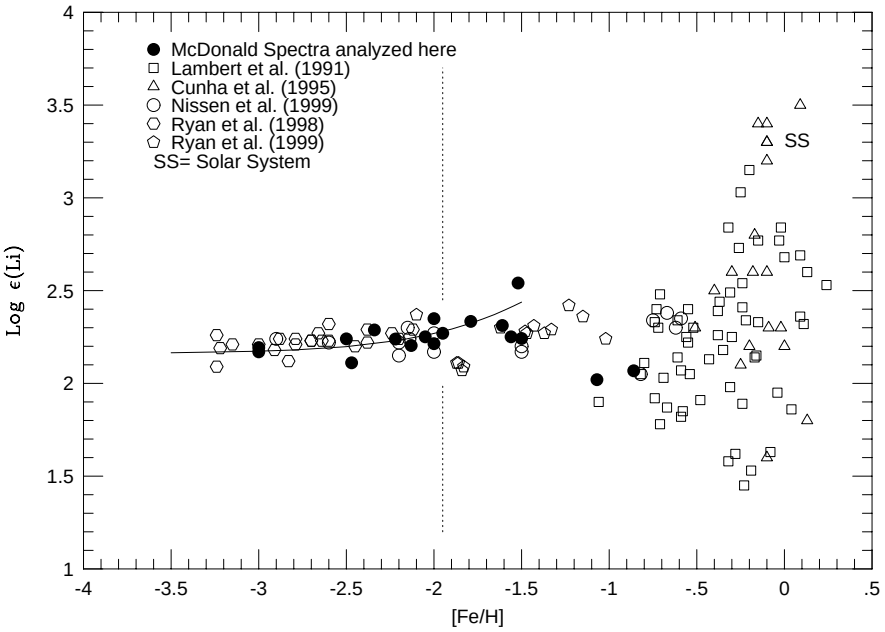

Fig. 11. Lithium abundances, log ϵ(Li) $\equiv$ [Li] $\equiv$ 12+log(Li/H) versus metallicity (on a log scale relative to solar) from a compilation of stellar observations by V. V. Smith. The solid line is intended to guide the eye to the "Spite Plateau".

12+log(Li/H)) for $-3.5 \leq$ [Fe/H] ≤ -1, and they derive a primordial abundance of $[\mathrm{Li}]_\mathrm{P} \approx 2.0-2.1$. This abundance is low compared to the value found by Thorburn[35], who derived $[\mathrm{Li}]_\mathrm{P} \approx 2.25 \pm 0.10$. The stellar temperature scale plays a key role in using the observed equivalent widths to derive the ^{7}Li abundance. Studies of halo and Galactic Globular Cluster stars employing the infrared flux method effective temperature scale suggest a higher lithium plateau abundance[36]: $[\mathrm{Li}]_\mathrm{P} = 2.24 \pm 0.01$, similar to Thorburn's[35] value. Recently, Melendez & Ramirez[37] reanalyzed 62 halo dwarfs using an improved infrared flux method effective temperature scale. While they failed to confirm the [Li] – [Fe/H] correlation claimed by Ryan *et al.*[34], they suggest an even higher relic lithium abundance: $[\mathrm{Li}]_\mathrm{P} = 2.37 \pm 0.05$. A very detailed and careful reanalysis of extant observations with great attention to systematic uncertainties and the error budget has been done by Charbonnel and Primas[38], who find no convincing evidence for a Li trend with metallicity, deriving $[\mathrm{Li}]_\mathrm{P} = 2.21 \pm 0.09$ for their full sample and $[\mathrm{Li}]_\mathrm{P} = 2.18 \pm 0.07$ when they restrict their sample to unevolved (dwarf) stars. They suggest the Melendez & Ramirez value should be corrected downwards by 0.08 dex to account for different stellar atmosphere

models, bringing it into closer agreement with their results. To err on the side of conservatism, the lithium abundance of Melendez & Ramirez[37], $[\mathrm{Li}]_\mathrm{P} = 2.37 \pm 0.05$, which is closer to the SBBN expectation, will be adopted in further comparisons.

There is tension between the SBBN predicted relic abundance of ^{7}Li ($[\mathrm{Li}]_\mathrm{P} = 2.65^{+0.05}_{-0.06}$; see §2.2) and that derived from recent observational data ($[\mathrm{Li}]_\mathrm{P} = 2.37 \pm 0.05$). Systematic errors may play a large role confirming or resolving this factor of two discrepancy. The role of the stellar temperature scale has already been mentioned. Another concern is associated with the temperature structures of the atmospheres of these very cool, metal-poor stars. This can be important because a large ionization correction is needed since the observed neutral lithium is a minor component of the total lithium. Furthermore, since the low metallicity, dwarf, halo stars used to constrain primordial lithium are among the oldest in the Galaxy, they have had the most time to alter (by dilution and/or destruction) their surface lithium abundances, as is seen to be important for many of the higher metallicity stars shown in Fig. 11. While mixing stellar surface material to the interior would destroy or dilute any prestellar lithium, the very small observed dispersion among the lithium abundances in the low metallicity halo stars (in contrast to the very large spread for the higher metallicity stars) suggests this correction may not be large enough ($\lesssim 0.1 - 0.2$ dex at most) to bridge the gap between theory and observation; see, *e.g.*, Pinsonneault *et al.*[39] and further references therein.

4. Discussion

The cosmic nuclear reactor was active for a brief epoch in the early evolution of the universe. As the Universe expanded and cooled the nuclear reactor shut down after $\sim$ 20 minutes, having synthesized in astrophysically interesting abundances only the lightest nuclides D, ^{3}He, ^{4}He, and ^{7}Li. For the standard models of cosmology and particle physics (SBBN) the relic abundances of these nuclides depend on only one adjustable parameter, the baryon abundance parameter η_B (the post-$e^\pm$ annihilation value of the baryon (nucleon) to photon ratio). If the standard models are the correct description of the physics controlling the evolution of the universe, the abundances of the four nuclides should be consistent with a single value of η_B and this baryon density parameter should also be consistent with the values inferred from the later evolution of the universe (*e.g.*, at present as well as $\sim$ 400 kyr after BBN, when the relic photons left their imprint on the CBR observed by WMAP and other detectors). There are, however, two other particle physics related cosmological parameters, the lepton asymmetry parameter ξ_e and the expansion rate parameter S, which can affect the BBN-predicted relic abundances. For SBBN it is assumed that $\xi_e = 0$ and $S = 1$. Deviations of either or both of these parameters from their standard model expected values could signal new physics beyond the standard model(s).

The simplest strategy is to test first the predictions of SBBN. Agreement between theory and observations would provide support for the standard models.

Disagreements are more difficult to interpret in that while they may be opening a window on new physics, they may well be due to unaccounted for systematic errors along the path from observations of post-BBN material to the inferred primordial abundances. Subject to this latter caveat, the confrontation between theory and data can provide useful limits to (some of) the parameters associated with new physics which complement those from high precision, terrestrial experiments. In the comparisons presented below, the abundances (and their inferred uncertainties) presented in §3 are adopted and compared to the BBN predictions described by the simple fits from §2.2. For ^{4}He the SSBN range in $\eta_{\rm B}$ favored by the adopted primordial abundance lies outside the range of validity of the simple fit; for ^{4}He and SBBN, the best fit and uncertainty in $\eta_{\rm B}$ is derived from the more detailed BBN calculations. While not all models of new physics proposed in the literature can be tested in this manner, this approach does offer the possibility of constraining a large subset of them and of providing a useful framework for understanding qualitatively how many of the others might affect the BBN predictions.

4.1. *SBBN*

The discussion in §3 identifies a set of primordial abundances. Since these choices are certainly subjective and likely to change as more data are acquired, along with a better understanding of and accounting for systematic errors, the analytic fits presented in §2.2 can be very useful in relating new conclusions and constraints to those presented here. The abundances and nominal 1σ uncertainties adopted here are: $y_{\rm D} = 2.6 \pm 0.4$, $y_3 = 1.1 \pm 0.2$, $\rm Y_P = 0.241 \pm 0.004$, and $y_{\rm Li} = 2.34^{+0.29}_{-0.25}$ ($\rm [Li]_P = 2.37 \pm 0.05$). $\rm Y_P \leq 0.254$ is adopted for an upper bound (at $\sim 2\sigma$) to the primordial ^{4}He mass fraction. The corresponding SBBN values of the baryon density parameter are shown in Figure 12, along with that inferred from the CBR and observations of Large Scale Structure[2] (labelled WMAP).

As Figure 12 reveals, the adopted relic abundances of D and ^{3}He are consistent with the SBBN predictions ($\eta_{\rm D} = 6.1 \pm 0.6$, $\eta_{^3{\rm He}} = 6.0 \pm 1.7$) and both are in excellent agreement with the non-BBN value[2] ($\eta_{\rm WMAP} = 6.14 \pm 0.25$). If the most recent deuterium abundance determination in a high redshift, low metallicty QSOALS[18] is included in estimating the relic D abundance, the mean shifts to a slightly lower value ($y_{\rm D} = 2.4 \pm 0.4$), corresponding to a slightly higher estimate for the baryon density parameter ($\eta_{\rm D} = 6.4 \pm 0.7$), which is still consistent with ^{3}He and with WMAP. Were it not for the very large dispersion among the D abundance determinations (see §3.1), the formal error in the mean ($\sim 5\%$) could have been adopted for the uncertainty in $y_{\rm D}$, leading to a $\sim 3\%$ determination of $\eta_{\rm D}$, competitive with that from WMAP. Due to the very large observational and evolutionary uncertainties associated with ^{3}He, its abundance mainly provides a consistency check at present. Since the variations of its predicted relic abundance with S and ξ_e are similar to those for D, ^{3}He will not add new information to that from D in the comparisons to be discussed below.

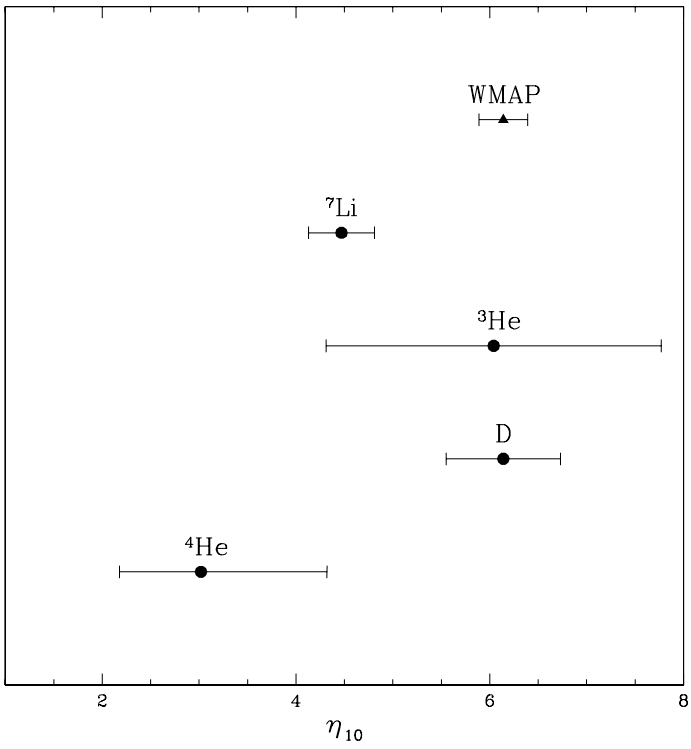

Fig. 12. The SBBN values for the early universe ($\sim$ 20 minutes) baryon abundance parameter η_{10} inferred from the adopted primordial abundances of D, ^{3}He, ^{4}He, and ^{7}Li (see §3.1-3.4). Also shown is the WMAP-derived CBR and LSS value ($\sim$ 400 kyr).

In addition to the successes of D and ^{3}He, Figure 12 exposes a tension between WMAP (and D and ^{3}He) and the adopted primordial abundances of ^{4}He and ^{7}Li. The 1σ range determined from ^{4}He is low: $2.2 \leq \eta_{\rm He} \leq 4.3$; however, the 2σ range is much larger: $1.7 \leq \eta_{\rm He} \leq 6.4$, encompassing the WMAP-inferred baryon density. The ^{7}Li inferred baryon density is also low ($\eta_{\rm Li} = 4.5 \pm 0.3$) and here the adopted errors appear to be far too small to bridge the gap to D and WMAP. These tensions may be a sign of systematic errors introduced when the observational data is used to derive the inferred primordial abundances or, it could be a signal of new physics beyond the standard models of cosmology and particle physics.

4.2. *Lithium*

As identified above, the SBBN abundances of D and ^{3}He are in agreement with each other and with the non-BBN estimate of the baryon density parameter from Large Scale Structure and the CBR. However, while the inferred primordial abundance

of ^{4}He is less than 2σ away from the SBBN-predicted value, that of lithium differs from expectations by a factor of ~ 2 (or more). It is unlikely that this conflict can be resolved through a non-standard expansion rate ($S \neq 1$) or a non-zero lepton number ($\xi_e \neq 0$). The reason is that in the $S - \eta_{\rm B}$ and $\xi_e - \eta_{\rm B}$ planes the isoabundance curves for D and ^{7}Li are very nearly parallel (see eqs. 16 & 23 in §2.2 and Figs. 1 & 2 from Kneller & Steigman[9]), so that once $y_{\rm D}$ is constrained, there is very little freedom to modify $y_{\rm Li}$. This may be seen by combining eqs. 16 & 23 to relate $\eta_{\rm Li}$ to $\eta_{\rm D}$,

$$\eta_{\rm Li} = \eta_{\rm D} + 3[(S-1) - \xi_e]. \tag{27}$$

Thus, for $\eta_{\rm D} \gtrsim 6$ and $|S-1| \lesssim 0.1$, $|\xi_e| \lesssim 0.1$, $\eta_{\rm Li} \approx \eta_{\rm D} \gtrsim 6$, so that $y_{\rm Li} \gtrsim 4$ ($[{\rm Li}]_{\rm P} \gtrsim 2.6$).

Nonetheless, a non-standard physics explanation of the lithium conflict is not ruled out. Indeed, there are models where late-decaying, massive particles reinitiate BBN, modifying the abundances of the light nuclides produced during the first 20 minutes. For an extensive, yet likely incomplete list (with apologies) of references, see Ref. [36] and further references therein. In such models it is quite possible to *reduce* the original BBN abundance of ^{7}Li to bring it into agreement with the value inferred from the observational data[34,35,36,37]. However, it is found that when the many new parameters available to these models are adjusted to achieve this agreement, the modified relic abundance of ^{3}He is much too large (see, *e.g.*, Ellis, Olive, and Vangioni[40]).

The difficulty in reconciling the observed and predicted relic abundances of ^{7}Li suggests that the problem may be in the stars. It is not at all unexpected that the very old halo stars where lithium is observed will have modified their original surface abundances, ^{7}Li in particular (see Pinsonneault *et al.*[39] and Charbonnel and Primas[38] for discussions and many additional references). While there is no dearth of physical mechanisms capable of destroying or diluting surface lithium, many of which are supported by independent observational data, the challenge has been to account for the required depletion (factor of 2 – 3) while maintaining a negligible dispersion ($\lesssim 0.1$ dex) among the "Spite plateau" lithium abundances.

Another possibility for reconciling the observed and predicted relic abundances of ^{7}Li lies in the nuclear physics. After all, given the estimates of uncertainties in the cross sections of the key nuclear reactions leading to the production and destruction of mass-7, the BBN-predicted abundance of ^{7}Li is the most uncertain ($\sim 10-20\%$) of all the light nuclides. Perhaps the conflict between theory and observation is the result of an error in the nuclear physics. This possibility was investigated by Cyburt, Fields, and Olive[41] who noted that some of the same nuclear reactions of importance in BBN, play a role in the standard solar model and are constrained by its success in accounting for the observed flux of solar neutrinos. While the uncertainty of a key nuclear reaction ($^3{\rm He}(\alpha,\gamma)^7{\rm Be}$) is large ($\sim 30\%$), it is far smaller than the factor of ~ 3 needed to reconcile the predicted and observationally inferred abundances[41].

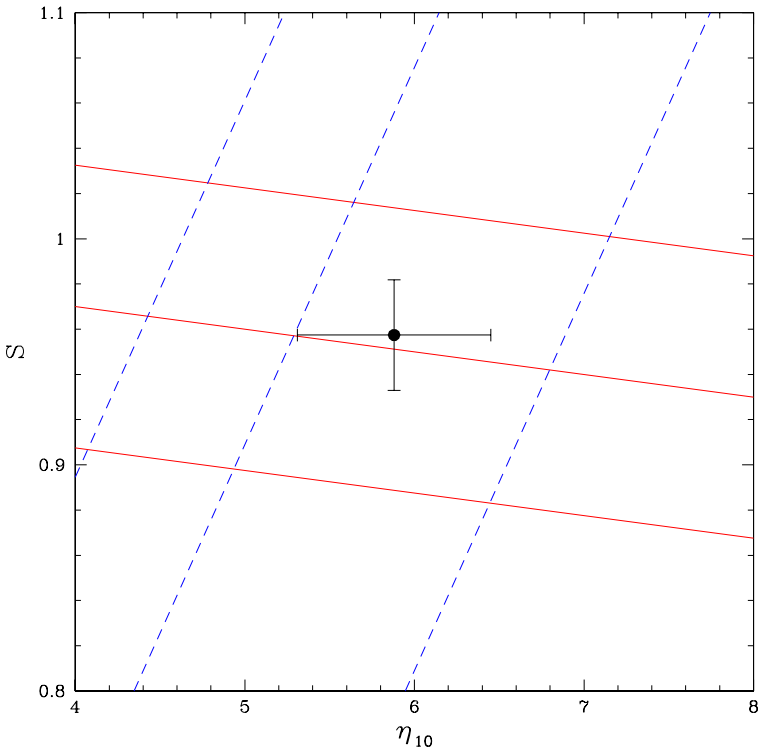

Fig. 13. The D and ^{4}He isoabundance curves in the $S - \eta_{10}$ plane, as in Fig. 2. The best fit point and the error bars correspond to the adopted primordial abundances of D and ^{4}He.

Considering the current state of affairs (no successful resolution based on new physics; possible reconciliation based on stellar astrophysics), ^{7}Li is not used below where the adopted relic abundances of D and ^{4}He are employed to set constraints on S and/or ξ_e.

4.3. *Non-Standard Expansion Rate: $S \neq 1$ ($\xi_e = 0$)*

If the lepton asymmetry is very small, of order the baryon asymmetry, then BBN depends on only two free parameters, $\eta_{\rm B}$ and S (or $\rm N_\nu$). Since the primordial abundance of D largely probes $\eta_{\rm B}$ while that of ^{4}He is most sensitive to S (see Fig. 2 and eqs. 16 & 20), for each pair of $y_{\rm D}$ and $\rm Y_P$ values (within reason) there will be a corresponding pair of $\eta_{\rm B}$ and S values. For the D and ^{4}He abundances adopted above ($y_{\rm D} = 2.6 \pm 0.4$, $\rm Y_P = 0.241 \pm 0.004$) the best fits for $\eta_{\rm B}$ and S, shown in Figure 13, are for $\eta_{10} = 5.9 \pm 0.6$ and $S = 0.96 \pm 0.02$; the latter corresponds to $\rm N_\nu = 2.5 \pm 0.3$. These values are completely consistent with those inferred from the joint constraints on S and $\eta_{\rm B}$ from WMAP[42].

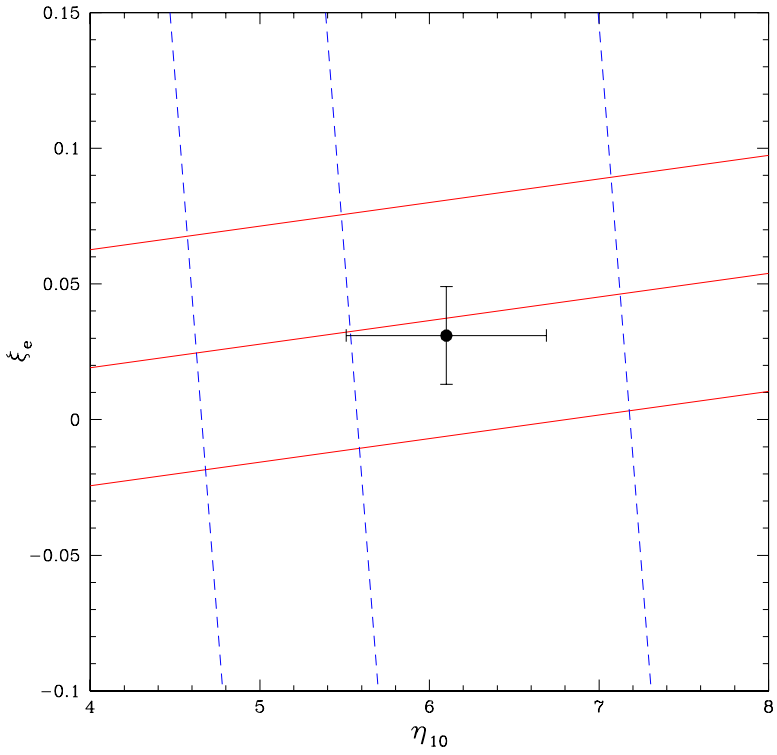

Fig. 14. The D and ^{4}He isoabundance curves in the $\xi_e - \eta_{10}$ plane, as in Fig. 3. The best fit point and the error bars correspond to the adopted primordial abundances of D and ^{4}He.

As expected from the discussion in §2.2, the lithium abundance is largely driven by the adopted deuterium abundance and is little affected by the small departure from the standard expansion rate. For the above best fit values, $y_{\rm Li} = 4.3 \pm 0.9$ ($[{\rm Li}]_{\rm P} = 2.63^{+0.08}_{-0.10}$). This class of non-standard models ($S \neq 1$), while reconciling ^{4}He with D and with the CBR, is incapable of resolving the lithium conflict.

4.4. *Non-Zero Lepton Number: $\xi_e \neq 0$ ($S = 1$)*

While most popular extensions of the standard model which attempt to account for neutrino masses and mixings suggest a universal lepton asymmetry comparable in magnitude to the baryon asymmetry ($\xi_e \sim O(\eta_{\rm B}) \lesssim 10^{-9}$)[f], there is no direct evidence that nature has made this choice. Although the CBR is blind to a relatively

[f]By charge neutrality the charged lepton excess is equal to the proton excess which constitutes $\gtrsim 87\%$ of the baryon excess. Therefore, any significant lepton asymmetry ($\xi_e >> \eta_{\rm B}$) must be hidden in the unobserved relic neutrinos.

small lepton asymmetry, BBN provides an indirect probe of it[43]. As discussed in §1.3 & §2, a lepton asymmetry can change the neutron to proton ratio at BBN, modifying the light element yields, especially that of ^{4}He. Assuming $S = 1$ and allowing $\xi_e \neq 1$, BBN now depends on the two adjustable parameters $\eta_{\rm B}$ and ξ_e which may be constrained by the primordial abundances of D and ^{4}He. Given the strong dependence of $Y_{\rm P}$ on ξ_e and of $y_{\rm D}$ on $\eta_{\rm B}$, these nuclides offer the most leverage. In Figure 14 are shown the D and ^{4}He isoabundance curves (*i.e.*, the fits from §2.2) in the $\xi_e - \eta_{\rm B}$ plane, along with the best fit point (and its 1σ uncertainties) determined by the adopted primordial abundances. The best fit baryon abundance, $\eta_{10} = 6.1 \pm 0.6$ is virtually identical to the SBBN (and WMAP) value. While the best fit lepton asymmetry, $\xi_e = 0.031 \pm 0.018$, is non-zero, it differs from zero by less than 2σ (as it should since the adopted value of $Y_{\rm P}$ differs from the SBBN expected value by less than 2σ).

As expected from the discussion above for $S \neq 1$ and in §2.2, here, too, the lithium abundance is largely driven by the adopted deuterium abundance and is little affected by the small lepton asymmetry allowed by D and ^{4}He. For the above best fit values, the predicted lithium abundance is virtually identical to the SBBN/WMAP and $S \neq 1$ values: $y_{\rm Li} = 4.3 \pm 0.9$ ($[{\rm Li}]_{\rm P} = 2.64^{+0.08}_{-0.10}$). A lepton asymmetry which reconciles ^{4}He with D cannot resolve the lithium conflict.

4.5. *An Example: Alternate Relic Abundances for D and ^{4}He*

It is highly likely that at least some of the tension between D and ^{4}He is due to errors associated with inferring their primordial abundances from the current observational data. As a result, in the future the abundances adopted here may be replaced by revised estimates. This is where the simple, analytic fits derived by KS[9] and presented in §2.2 can be of value to those who lack an in-house BBN code. Provided that the *revised* abundances lie in the ranges $2 \lesssim y_{\rm D} \lesssim 4$ and $0.23 \lesssim Y_{\rm P} \lesssim 0.25$, these fits will provide quite accurate, back of the envelope estimates of $\eta_{\rm B}$, S, ξ_e, and of $y_{\rm Li}$. As an illustration, let's revisit the discussion in §4.3 & §4.4, now adopting for D the weighted mean deuterium abundance which results when the most recent determination[18] is included, $y_{\rm D} = 2.4 \pm 0.4$ (see §3.1), along with, for ^{4}He, the helium abundance derived by applying the OS mean offset to the IT-inferred primordial value (see eq. 25) **without** the *icf*-correction, $Y_{\rm P} = 0.2472 \pm 0.0035$ (see §3.3). These alternate abundances correspond to $\eta_{\rm D} \approx 6.5 \pm 0.7$ and $\eta_{\rm He} \approx 5.5 \pm 2.2$.

For $\xi_e = 0$, the *new* values for the expansion rate factor and the baryon density parameter are $S = 0.991 \pm 0.022$ ($N_\nu = 2.9 \pm 0.3$) and $\eta_{10} = 6.4 \pm 0.6$. While the N_ν estimate is entirely consistent with $N_\nu = 3$, the corresponding $\sim 2\sigma$ upper bound ($N_\nu \lesssim 3.5$) still excludes even one extra light scalar. The baryon density parameter is slightly higher than, but entirely consistent with that inferred from the CBR. As anticipated from the previous discussion, the predicted lithium abundance hardly changes at all, but it does increase slightly to further exacerbate the conflict with the observationally inferred value, $y_{\rm Li} \approx 4.9 \pm 1.1$ ($[{\rm Li}]_{\rm P} = 2.69^{+0.09}_{-0.11}$).

For $S = 0$, the *new* values for the lepton asymmetry parameter and the baryon density parameter are $\xi_e = 0.007 \pm 0.016$ and $\eta_{10} = 6.5 \pm 0.7$. The former is consistent with no lepton asymmetry (*i.e.*, with $\xi_e \sim O(\eta_{\rm B})$) and the latter is slightly higher than, but still entirely consistent with the baryon density parameter inferred from the CBR. As expected, here, too, the predicted lithium abundance increases slightly from the already too large SBBN value, $y_{\rm Li} \approx 4.9 \pm 1.1$ ($[{\rm Li}]_{\rm P} = 2.69^{+0.09}_{-0.11}$).

4.6. *Other Non-Standard Models*

Although the parameterization of BBN in terms of S and ξ_e explored in the previous sections encompasses a large set of non-standard models of cosmology and particle physics, it by no means describes all interesting extensions of the standard model. As already mentioned, there is a class of models where BBN proceeds normally but a second epoch of early universe nucleosynthesis is initiated by the late decay of a massive particle[40]. Despite the fact that such models have many more free parameters, such as the mass, abundance, and lifetime of the decaying particle, the constraints imposed by the observationally inferred relic abundances of D, ^{3}He, ^{4}He, and ^{7}Li are sufficiently strong to challenge them (see, *e.g.*, Ellis, Olive & Vangioni[40]).

There are other models which cannot be simply described by the $\{\eta_{\rm B},\, S,\, \xi_e\}$ parameter set. In most cases they introduce several free parameters in addition to the baryon density parameter. Since there are only four nuclides whose relic abundances are reasonably constrained, the leverage of BBN on these models may be limited in some cases. A case in point is the class of models where the universe is inhomogeneous at BBN (IBBN); see the recent article by Lara[44] and the extensive references to earlier work therein. In IBBN the geometry of the inhomogeneities (spheres, cylinders, ...) is important, as are the scales of the imhomogeneities and their amplitudes (density contrasts). Nonetheless, even with all these adjustable parameters, except when they take on values indistinguishable from SBBN, IBBN models predict an excess of lithium (even more of an excess than for SBBN). This is inevitable since in IBBN ^{7}Li is overproduced in the low nucleon density regions and ^{7}Be is overproduced in the high density regions (see the multi-valued lithium abundance curve in Fig. 1).

5. Summary and Conclusions

As the early Universe evolved from hot and dense to cool and dilute, it passed through a short-lived epoch when conditions of temperature and density permitted the synthesis of astrophysically interesting abundances of D, ^{3}He, ^{4}He, and ^{7}Li. At present, observations of these nuclides in a variety of astrophysical sites (stars, Galactic and extragalactic H II regions, QSOALS, etc.) have permitted quite precise estimates of their primordial abundances, opening a window on early-universe cosmology and providing constraints on physics beyond the standard models of

cosmology and particle physics. The relic abundances of D, ^{3}He, and ^{7}Li are nuclear reaction rate limited, providing good probes of the nucleon density when the universe was less than a half hour old. This is complementary to baryon density estimates from the CBR, whose information was encoded some 400 kyr later, and to those provided by observations of the current or recent universe, 13 Gyr after BBN. Of these light nuclides, D is the baryometer of choice and current estimates of the relic abundance, $y_{\rm D} = 2.6 \pm 0.4$, suggest a baryon to photon ratio, unchanged from BBN to the present, of $\eta_{10} = 6.1 \pm 0.6$, in excellent agreement with the WMAP and LSS determined value of $\eta_{10} = 6.14 \pm 0.25$. For this choice ($S = 1$, $\xi_e = 0$), the less well constrained relic abundance of ^{3}He ($y_3 = 1.1 \pm 0.2$)[24] is also in agreement with its SBBN expected value. These successes for the standard models are tempered by the challenges posed by ^{4}He and ^{7}Li. The SBBN predicted ^{4}He mass fraction, $\rm Y_P = 0.248$, differs from the observationally inferred primordial abundance adopted here, $\rm Y_P = 0.241 \pm 0.004$, by nearly 2σ. However, as discussed in §3.3, the uncertainties in $\rm Y_P$ are likely dominated by systematic, not statistical errors, so it is difficult to know if this tension between D (and ^{3}He and the CBR) and ^{4}He is cause for serious concern. In contrast to the other light nuclides, the BBN abundance of ^{4}He is insensitive to the nuclear reaction rates and, hence, to the nucleon density at BBN. $\rm Y_P$ is largely set by the neutron to proton ratio at BBN, so that ^{4}He is an excellent probe of the weak interactions and of the early Universe expansion rate. Perhaps the ^{4}He challenge to SBBN is a signal of new physics. The SBBN predicted abundance of ^{7}Li ($[{\rm Li}]_{\rm P} = 2.65^{+0.05}_{-0.06}$) is nearly a factor of two higher than the observationally determined value[37] ($[{\rm Li}]_{\rm P} = 2.37 \pm 0.05$). While there is some spread in the lithium abundances inferred from the data[38], the largest cause for concern is that Li is observed in the oldest stars in the Galaxy, which have had ample time to modify their original surfaces abundances. For ^{7}Li, it appears likely that astrophysical uncertainties dominate at present.

Thus, while there appears to be qualitative confirmation of the standard models of cosmology and particle physics extrapolated back to the first seconds of the evolution of the Universe, precision should not be confused with accuracy. The accuracy of the presently-inferred primordial abundances of D, ^{3}He, ^{4}He, and ^{7}Li remains in question and it would not be at all surprising if one or more of them changed by more than the presently-quoted errors. After all, there are only 5 (6) lines of sight where deuterium is observed in high-redshift, relatively unprocessed (low metallicity) material; ^{3}He is only observed in the chemically processed interstellar medium of the Galaxy and the lack of variation of its abundance with metallicity or with position in the Galaxy suggest a very delicate balance between post-BBN production, destruction and survival; systematic errors and corrections to the ^{4}He abundance inferred from observations of low metallicity, extragalactic H II regions are likely larger, maybe much larger, than the current statistical uncertainties; lithium is derived from observations of very old, very low metallicity stars (good!) in our Galaxy (bad?) and the corrections for stellar atmosphere models

and, especially, for main sequence mixing-induced depletion and destruction remain large and uncertain. Much interesting, important work remains for observational and theoretical astronomers.

The current standard models receive strong support from these messengers from the early universe, confirming in broad outline our understanding of the evolution of the Universe and the particles in it, from the first seconds to the present. Any models of new physics must consider this success and avoid introducing new conflicts. Much interesting, important work remains for cosmologists and high energy theorists.

Acknowledgments

I am grateful to all those I've collaborated with over the years on the subject of this review. Discussions with J. E. Felten, K. A. Olive, E. D. Skillman, M. Tosi, D. Tytler, and J. K. Webb were especially valuable in its preparation. My research is supported by a grant (DE-FG02-91ER40690) from the US Department of Energy.

References

1. G. Steigman, *Ann. Rev. Astron. and Astrophys.* **14**, 339 (1976).
2. D. N. Spergel *et al.*, *ApJS* **148**, 175 (2000).
3. L. Randall and R. Sundrum, *Phys. Rev. Lett.* **83**, 3370 (1999); Phys. Rev. Lett. **83**, 4690 (1999).
4. J. P. Kneller and G. Steigman, *Phys. Rev. D* **67**, 063501 (2003).
5. J. D. Barrow and R. J. Scherrer, *Phys. Rev. D* **70**, 103515 (2004).
6. G. Steigman, D. N. Schramm, J. E. Gunn, *Phys. Lett. B*, **66**, 202 (1977).
7. M. Kawasaki, K. Kohri, N. Sugiyama, *Phys. Rev. Lett.* **82**, 4168 (1999); S. Hannestad, *Phys. Rev. D* **70**, 043506 (2004).
8. C. Lunardini and A. Y. Smirnov, *Phys. Rev. D*, **64**, 073006 (2001); A. D. Dolgov, S. H. Hansen, S. Pastor, S. T. Petcov, G. G. Raffelt, D. V. Semikoz, *Nucl. Phys. B*, **632**, 363 (2002); Y. Y. Wong, *Phys. Rev. D*, **66**, 025015 (2002); K. N. Abazajian, J. F. Beacom, N. F. Bell, *Phys. Rev. D*, **66**, 013008 (2002).
9. J. P. Kneller and G. Steigman (KS), *New J. Phys.* **6**, 117 (2004).
10. H.-S. Kang and G. Steigman. *Nucl. Phys. B* **372**, 494 (1992).
11. S. Burles, K. M. Nollett, M. S. Turner (BNT), *Phys. Rev. D* **63**, 063512 (2001).
12. A. Serebrov, *et al.*, *Phys. Lett. B* **605**, 72 (2005).
13. N. Hata, R. J. Scherrer, G. Steigman, D. Thomas, T. P. Walker, S. Bludman, P. Langacker, *Phys. Rev. Lett.* **75**, 3977 (1995).
14. E. Vangioni-Flam, K. A. Olive, B. D. Fields, M. Cassé, *ApJ* **585**, 611 (2003).
15. R. Epstein, J. Lattimer, D. N. Schramm, *Nature* **263**, 198 (1976).
16. D. Kirkman, D. Tytler, N. Suzuki, J. O'Meara, D. Lubin, *ApJS* **149**, 1 (2003).
17. G. Steigman, *MNRAS* **269**, L53 (1994).
18. N. H. M. Crighton, J. K. Webb, A. Ortiz-Gil, A. Fernández-Soto, *MNRAS* **355**, 1042, (2004).
19. B. T. Draine, preprint (to appear in *Astrophysics in the Far Ultraviolet*), astro-ph/0410310 (2004).
20. I. Iben, Jr., *ApJ* **147**, 624 (1967); R. T. Rood, *ApJ* **177**, 681 (1972); D. S. P. Dearborn, D. N. Schramm, G. Steigman, *ApJ* **203**, 35 (1986); E. Vassiliadis and P. R. Wood, *ApJ* **413**, 641 (1993); D. S. P. Dearborn, G. Steigman, M. Tosi, *ApJ* **465**, 887 (1996) (erratum: *ApJ* **473**, 570).

21. I.-J. Sackmann and A. I. Boothroyd, *ApJ* **510**, 217 (1999); *ibid ApJ* **510**, 232 (1999).
22. R. T. Rood, G. Steigman, B. M. Tinsley, *ApJL* **207**, L57 (1976); K. A. Olive, R. T. Rood, D. N. Schramm, J. Truran, E. Vangioni-Flam, *ApJ* **444**, 680 (1995); D. S. P. Dearborn, G. Steigman, M. Tosi, *ApJ* **465**, 887 (1996) (erratum: *ApJ* **473**, 570); D. Galli, L. Stanghellini, M. Tosi, F. Palla, *ApJ* **477**, 218 (1997); K. A. Olive, D. N. Schramm, S. T. Scully, J. Truran, *ApJ* **479**, 752 (1997); F. Palla, R. Bachiller, L. Stanghellini, M. Tosi, D. Galli, *A&A* **355**, 69 (2000); C. Chiappini, A. Renda, F. Matteucci, *A&A* **395**, 789 (2002).
23. R. T. Rood, T. M. Bania, D. S. Balser, T. L. Wilson, *Space Sci. Rev.* **84**, 185 (1998); J. Geiss, J., G. Gloeckler, *Space Sci. Rev.* **84**, 239 (1998).
24. T. M. Bania, R. T. Rood, D. S. Balser (BRB): *Nature* **415**, 54 (2002).
25. D. Romano, M. Tosi, F. Matteucci, C. Chiappini, *MNRAS* **346**, 295 (2003).
26. Y. I. Izotov and T. X. Thuan (IT), *ApJ* **500**, 188 (1998); *ibid*, *ApJ* **602**, 200 (2004).
27. K. Davidson and T. D. Kinman, *ApJ* **58**, 321 (1985).
28. J. Lequeux, M. Peimbert, J.F. Rayo, A. Serrano, S. Torres-Peimbert, *A&A* **80**, 155 (1979); B. E. J. Pagel, E. A. Simonson, R.J. Terlevich, M. G. Edmunds, *MNRAS* **255**, 325 (1992); K. A. Olive, E. D. Skillman, G. Steigman, *ApJ* **489**, 1006 (1997).
29. K. A. Olive and E. D. Skillman, *New A* **6**, 119 (2001); K. A. Olive, E. D. Skillman (OS) *ApJ* **617**, 29 (2004).
30. M. Peimbert, A. Peimbert, M. T. Ruiz, *ApJ* **541**, 688 (2000); A. Peimbert, M. Peimbert, V. Luridiana, *ApJ* **565**, 668 (2002).
31. G. Steigman, S. M. Viegas, R. Gruenwald *ApJ* **490**, 187 (1997).
32. S. M. Viegas, R. Gruenwald, G. Steigman, *ApJ* **531**, 813 (2000); R. Gruenwald, G. Steigman, S. M. Viegas (GSV), *ApJ* **567**, 931 (2002); D. Sauer and K. Jedamzik, *A&A* **381**, 361 (2002).
33. C. Esteban and M. Peimbert, *A&A* **300**, 87 (1995).
34. S. G. Ryan, J. E. Norris, T. C. Beers, *ApJ* **523**, 654 (1999); S. G. Ryan, T. C. Beers, K. A. Olive, B. D. Fields, J. E. Norris, *ApJ* **530**, L57 (2000).
35. J. A. Thorburn, *ApJ* **421**, 318 (1994).
36. P. Bonifacio, P. Molaro, *MNRAS* **285**, 847 (1997); P. Bonifacio, P. Molaro, L. Pasquini, *MNRAS* **292**, L1 (1997).
37. J. Melendez and I. Ramirez, *ApJL* **615**, L33 (2004).
38. C. Charbonnel and F. Primas, *A&A* **442**, 961 (2005).
39. M. H. Pinsonneault, G. Steigman, T.P. Walker, V. K. Narayanan, *ApJ* **574**, 398 (2002).
40. M. H. Reno and D. Seckel, *Phys. Rev. D* **37**, 3441 (1988); S. Dimopoulos, R. Esmailzadeh, L. J. Hall, G. D. Starkman, *ApJ* **330**, 545 (1988); J. A. Frieman, E. W. Kolb, M. S. Turner, *Phys. Rev. D* **41**, 3080 (1990); K. Jedamzik, *Phys. Rev. Lett.* **84**, 3248 (2000); *ibid*, *Phys. Rev. D* **70**, 063524, 083510 (2004); J. L. Feng, A. Rajaraman, F. Takayama, *Phys. Rev. D* **68**, 063504 (2003); J. L. Feng, S. Su, F. Takayama, *Phys. Rev. D* **70**, 0635014 (2003); J. L. Feng, S. Su, F. Takayama, *Phys. Rev. D* **70**, 075019 (2003); R. H. Cyburt, J. R. Ellis, B. D. Fields, K. A. Olive, *Phys. Rev. D* **67**, 103521, (2003); M. Kawasaki, K. Kohri, T. Moroi, *Phys. Rev. D* **71**, 083502, (2005); J. Ellis, K. A. Olive, E. Vangioni, *Phys. Lett B* **619**, 30 (2005).
41. R. H. Cyburt, B. D. Fields, K. A. Olive, *Phys. Rev. D* **69**, 123519 (2004).
42. V. Barger, J. P. Kneller, H.-S. Lee, D. Marfatia, G. Steigman, *Phys. Lett. B* **566**, 8 (2003).
43. V. Barger, J. P. Kneller, D. Marfatia, P. Langacker, G. Steigman, *Phys. Lett. B* **569**, 123 (2003).
44. J. F. Lara, *Phys.Rev. D* **72**, 023509 (2005).